ΣΧΟΛΗ ΘΕΤΙΚΩΝ ΕΠΙΣΤΗΜΩΝ

ΤΜΗΜΑ ΦΥΣΙΚΗΣ

ΧΡΟΝΙΚΟΣ ΧΑΡΑΚΤΗΡΙΣΜΟΣ ΣΤΕΝΟΥ ΠΑΛΜΟΥ ΥΠΕΡΘΕΣΗΣ ΧΑΜΗΛΗΣ ΤΑΞΗΣ ΑΡΜΟΝΙΚΩΝ ΛΕΙΖΕΡ

ΣΚΑΝΤΖΑΚΗΣ ΕΜΜΑΝΟΥΗΛ

ΜΕΤΑΠΤΥΧΙΑΚΗ ΕΡΓΑΣΙΑ

ΥΠΕΥΘΥΝΟΣ ΚΑΘΗΓΗΤΗΣ: ΔΗΜΗΤΡΗΣ ΧΑΡΑΛΑΜΠΙΔΗΣ

ΥΠΕΥΘΥΝΟΣ ΕΡΕΥΝΗΤΗΣ: ΤΖΑΛΛΑΣ ΠΑΡΗΣ

ΗΡΑΚΛΕΙΟ, ΜΑΡΤΙΟΣ 2007

Χρονικος Χαρακτηρισμος Στενου Παλμου Υπερθεσης Χαμηλης Ταξεις Αρμονικων Λειζερ

Σκαντζακης Εμμανουηλ

Μεταπτυχιακη Εργασια

Υπευθυνος Καθηγητης: Δημητρης χαραλαμπιδης
Υπευθυνος ερευνητης: τζαλλας παρις

Ηρακλειο, μαρτιος 2007

Temporal Characterization Of A Short Pulse Synthesized By The Superposition Of Low Order Harmonics

Skantzakis Emmanouil

Master Thesis

Thesis Supervisors: D. Charalambidis, P. Tzallas

Heraclion, March 2007

Ευχαριστίες

Η εργασία αυτή είναι αποτέλεσμα της συνεργασίας μιας ομάδας ανθρώπων τους οποίους θα ήθελα να ευχαριστήσω.

Αρχικά, θα ήθελα να ευχαριστήσω ιδιαίτερα τον κ. Δημήτρη Χαραλαμπίδη, Καθηγητή του Τμήματος Φυσικής της σχολής Θετικών Επιστημών του Πανεπιστημίου Κρήτης, για την πολύτιμη συνεργασία μας κατά τη διάρκεια εκπόνησης της εργασίας αυτής καθώς και για την γενικότερη εποπτεία της. Χάρις σε αυτόν μου δόθηκε η ευκαιρία να ασχοληθώ με τον τομέα της Ατομικής Φυσικής πολύ ισχυρών πεδίων ενώ παράλληλα μου άνοιξε τους επιστημονικούς μου ορίζοντες και με έκανε να δω την εργασία αυτή σαν μία πρόκληση.

Ένα μεγάλο ευχαριστώ θα ήθελα να εκφράσω στον Δρ. Πάρη Τζάλλα, Ερευνητή Δ' του Ινστιτούτου Ηλεκτρονικής Δομής και Λέιζερ του Ιδρύματος Τεχνολογίας και Έρευνας του οποίου η επιστημονική καθοδήγηση υπήρξε για μένα πραγματικά ουσιαστική. Τον ευχαριστώ ιδιαίτερα για την ενθαρρυντική του στάση. Οι ατελείωτες ώρες συζητήσεων που πραγματοποιήθηκαν μεταξύ μας προκειμένου να γίνουν κατανοητές κάποιες πτυχές αυτής της εργασίας, τον οποίο πρέπει να ομολογήσω ότι πολλές φορές τον έφθαναν σε σημείο εξάντλησης, ήταν μία εμπειρία και μαζί του έμαθα πώς να αντιμετωπίζω προβλήματα μου φάνταζαν άλυτα (ή λυμένα ενώ δεν ήταν). Ένα μεγάλο κομμάτι της εργασίας δεν θα είχε πραγματοποιηθεί αν δεν ήταν αυτός.

Επίσης θα ήθελα να εκφράσω Δρ. Μανώλη Μπενή τις ευχαριστίες μου για τις πολύτιμες συμβουλές του για θέματα πειραματικού κενού. Στις κρίσιμες στιγμές ήταν πάντα εκεί για να με βοηθήσει σε ότι χρειαζόμουν.

Επίσης θα ήθελα να ευχαριστήσω την κα. Αντωνία Μπονάρου για την καθημερινή συντήρηση αλλά και επίλυση των προβλημάτων του λέιζερ.

Ιδιαίτερα θα ήθελα να ευχαριστήσω ιδιαίτερα τον Γρηγόρη Μαραβέλια για την ενθαρρυντική του στάση κατά την διάρκεια αυτής της διπλωματικής. Περάσαμε πολύ ωραίες αλλά και δύσκολες στιγμές τόσο εντός όσο και εκτός εργαστηρίου.

Δεν θα πρέπει να παραλείψω να εκφράσω τις ευχαριστίες μου σε όλους τους προπτυχιακούς, μεταπτυχιακούς φοιτητές και υποψηφίους διδάκτορες του εργαστηρίου των λέιζερ. Το φιλικό κλίμα το οποίο επικρατεί, κάνει την εργασία στο συγκεκριμένο χώρο πολύ πιο ευχάριστη και εποικοδομητική.

Τέλος ένα μεγάλο ευχαριστώ θα ήθελα να δώσω σε κάποιους άνθρωπους που με στήριξαν και με βοήθησαν με τον δικό τους τρόπο, **που δεν ήταν απαραίτητα επιστημονικός**, κατά την περίοδο πραγματοποίησης αυτής της διπλωματικής. Μπορεί μερικοί να έφυγαν και άλλοι να παρέμειναν αλλά να ξέρουν ότι πάντα θα είναι μαζί μου. Ονόματα δεν θα δωθούν γιατί ξέρουν πολύ καλά ποιοι είναι.

Ευχαριστώ ξανά όλους…

Σκαντζάκης Εμμανουήλ

Μάρτιος 2007

«Life on Earth is simple…enjoy the beauty…love…»

Anonymous

Abstract

Nowadays, it is well established that the superposition of higher-order harmonics (HOH), resulting from the non-linear response of matter to intense laser pulses (greater than 10^{13} W/cm^2), comprises an avenue towards ultra-short pulse generation reaching the attosecond time-scale. Although this field has progressed significantly there are still a number of difficulties one has to surmount. An arbitrary superposition of harmonics may not depict close temporal confinement. Thus, it is of great importance to know the temporal characteristics of the superposition.

Towards this goal an experimental method has been previously proposed the measurement of the relative phase distribution of the spectral components of a superposition of higher-order harmonics or the phase distribution of individual ones. This method is based on the "phase-control" principles of the excitation probability of an excited atom by the harmonic radiation and its fundamental frequency. The work of this thesis is focused on implementing this proposed method in order to directly measure the phase distributions of a short pulse produced by the superposition of the third and fifth harmonics of a Ti:Sapphire laser system generated in Xe gas. For In this measurement we used a previously proposed dispersionless experimental set-up based on a transmission grating interferometer. From the retrieved phase and the measured spectral amplitude distributions the temporal profile of the pulses could be reconstructed and was found in good agreement with the simulated one. This work opens-up a new route for the characterization of harmonics, for the temporal characterization of XUV pulses of ultra-short duration.

Contents

List of Figures

Chapter 1

Introduction

1.1 The femtosecond barrier

The measurement of short time intervals and the perception of the dynamics of ultra-fast phenomena are largely based on light pulses. The need for finer time resolution and the quest for higher peak power explain the continuous trend towards shorter laser pulses almost since the inception of the laser. The historical progress of ultra-short technology is summarized in **Figure 1.1-1**. The first pulsed lasers had durations of several hundreds of microseconds. Within a year or so, the invention of the Q-switch by Hellwarth (1961) reduced the pulse length to 100 ns, a three order of magnitude decrease. Mode-locking[1] accompanied by broad-gain dye laser media[2] further reduced the duration to less than 1 ps, another five orders of narrowing. The next reduction by three orders took another 10–15 years to be achieved. The main development was the ring cavity with intra-cavity prism compensation of the group velocity dispersion with which 6 fs pulses were produced, (Fork *et al* 1987) [3]. While the replacement of dyes by Ti–sapphire, a solid-state gain medium, brought considerable changes in the size, performance, reproducibility and ease of operation of ultra-short laser systems, the wavelength was at the same time shifted to the near infrared (800 nm), where 5 fs long pulses are just a few cycles long. By the end of the nineties, the innovations introduced by Kerr-lens mode-locking, self phase modulation spectral broadening, the availability of chirped, ultra-broad band mirrors and pulse compression all led to pulse lengths of about two full cycles (Steinmeyer *et al* 1999)[4]. Clearly, given that a pulse of light should be at least one cycle long and that the Ti–sapphire optical period is 2.7 fs, the necessary prerequisite for attosecond light pulses is higher carrier frequencies.

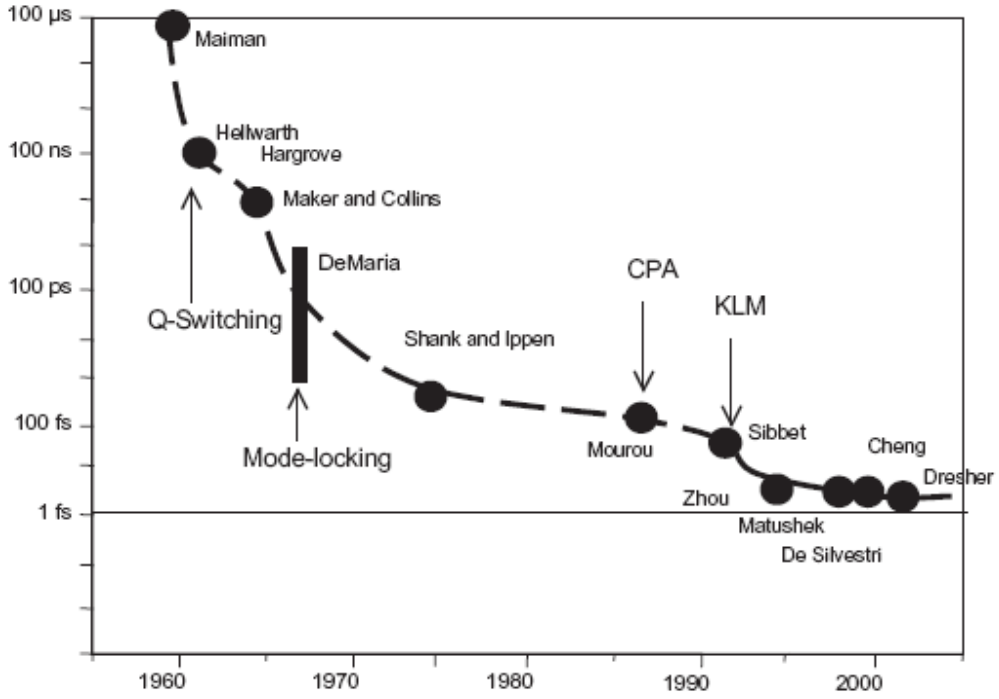

Figure 1.1-1: Temporal evolution of the laser pulse length evolution from the free-running laser of Maiman to the recent refinements. A few names and techniques mark the essential steps in this evolution. The existence a femtosecond barrier is clearly visible on the graph.

1.2 Beyond the barrier: attosecond x-ray pulses

During the last decade, a scheme was slowly emerging that had the potential to break the femtosecond barrier: Fourier synthesis (FS) could possibly generate a pulse of a few attoseconds (1 as = 10^{-18} s) and was proposed by Hansch (1990)[5], Farkas and Toth (1992)[6] and Harris *et al* (1993)[7]. The basic idea is the production of a comb of equidistant frequencies in the spectral domain with controlled relative phases, thus mimicking the operation of a modelocked laser. Hansch (1990)[5] proposed using sum and frequency mixing, while Farkas and Toth (1992)[6] recognized that high harmonic generation (HHG) could easily produce a broad spectral distribution in a series of lines separated by twice the fundamental frequency. Kaplan (1994)[8] suggested another physical effect for obtaining a broad series of equidistant frequencies: cascaded stimulated Raman scattering (CSRS), to which is related the concept subsequently developed by Harris and Sokolov (1997, 1998)[9,10]. Both the harmonic and Raman routes have now proved to be successful, and in the case of HHG pulses as short as 130 as can be synthesized (*Sansone et al* 2006)[11]. Clearly, the phase-locking of a periodic spectrum of equidistant frequencies can result only in a periodic intensity profile in the time

domain, i.e. a comb (or 'train') of pulses. The 'extraction' of a single pulse from such a train is in principle possible, although its period is only about 1 fs, i.e. too fast for the usual electronic devices.

Ivanov *et al* (1995)[12] and Platonenko and Strelkov (1999)[13] proposed achieving sub-femtosecond harmonic pulses from a 'long' pump pulse by taking advantage of the high sensitivity of HHG to the pump light polarization The first implemented autocorrelation technique used to confirm the existence of attosecond pulse trains from the superposition of high-order harmonics has been performed by Papadogiannis *et al.* (1999)[14]. A sub-femtosecond beating with a period of ~1.3 fs, was clearly observed, indicating the generation of sub-femtosecond XUV pulses. The resulted power spectrum showed up a modulation of $\sim 2\pi/\omega_L$ reflected the fact that harmonics were apart twice the frequency of the fundamental ω_L. Unlike the results and according to Corkum[15], "the production and measurement are entwined" pointing out that the measurement was not completely transparent, and a controversy, on its interpretation came in light[16],[17].

. Tcherbakov *et al* (2003)[18], Kovacev *et al* (2003)[19] have put these ideas to work. Alternatively the production of a single sub-femtosecond pulse by harmonic generation with a few-cycle pump pulse is possible: due to the high nonlinearity of the HHG process, a considerable temporal reduction of the harmonic pulse with respect to the pump is expected (and actually observed). *P. Tzallas et al.* (2003) who has recorded a second-order autocorrelation trace of a pulse train resulting from the coherent superposition of several harmonics - from the 7th to 15th[20], achieving of what was impossible till then. The non-linear signal detected was suitable for a second-order intensity autocorrelation showing an attosecond pulse train with pulses of duration 780 ± 80 as. In achieving this, a wave-front splitting arrangement, consisting of a spherical mirror cut into two halves controlled by a piezo-crystal translation stage, was used. The two parts of the bisected XUV pulse train were focused into a He gas-jet that was two-photon ionized. The ions were detected as a function of the displacement between the two half mirrors. Single pulses approaching 1 fs (Drescher *et al* 2001)[21], a few hundreds of attoseconds (Hentschel *et al* 2001)[22] and recently 250 as (Kienberger *et al* 2004)[23] were reported. These numbers give an idea of how fast the field is progressing.

To characterize attosecond pulses is quite a challenge. Besides their extremely short duration they have spectral components lying in the XUV spectral regime with rather low intensities. The latter comprised the major obstacle in using the standard short pulse

metrology such as second or higher order autocorrelation techniques by using non-linear crystals as well as because of their photon energies makes impossible the use of beam-splitters. The last few years many efforts have been directed towards new methods of pulse metrology. Some of them are based on cross-correlations between the harmonics and their source infrared (IR) field. These methods are able to provide information on the relative phase distribution between the harmonics, but they do not account for the frequency modulation (chirp) inside their bandwidth. The presence of the chirp could play a crucial role to their superposition and thus it should be taken into account.

An alternative way has been proposed in order to fully map out the phase distribution of the superimposed harmonics thus providing information also on the chirp within their bandwidth. The experimental implementation of the characterization of the third harmonic field is already achieved[24]. This method is based on what is known as phase-control of excitation processes. Furthermore, a suggested experimental arrangement has provided the appropriate tool for the implementation of this method by utilizing a freestanding transmission grating in order to overcome the problems of the absorption introduced by the beam-splitters[27].

1.3 The scope of this thesis

The motivation in this thesis is the implementation of the above proposed method utilizing the transmission grating interferometer in order to fully reconstruct the superposition of the third and the fifth harmonic pulse generated by a Ti:Sapphire laser. This work is considered as a first step for the full reconstruction of superposed higher order harmonics and corresponding attosecond pulses.

The thesis is organized as follows. Chapter 2 introduces the reader to the phase control technique which is the theoretical framework upon which our experimental work is based on.

Chapter 3 focuses on the implementation of this technique for the temporal characterization of the third harmonic (TH) and the fifth harmonic (FH). The experiment is fully simulated and the general concepts are presented. Furthermore, we present a ray-tracing analysis adapted to the used experimental set-up.

Chapter 4 includes a detailed description of the experimental set-up used. In Chapter 5, finally, we present the experimental results on utilizing this method as well as aspects for future experiments.

Chapter 2

The phase-control technique for the temporal characterization of the superposed 3rd and 5th harmonic field

In this Section, we apply the phase-control technique to a TH field (λ_3 = 267 nm) and a FH field (λ_5 = 160 nm) generated by a fundamental laser field with a central wavelength at 800 nm. This is to provide the theoretical framework upon which our experimental work is based on.

The mapping of a spectral phase distribution can be achieved by measuring the phase difference between all spectral components of the radiation to be characterized relative to a reference phase of a reference field, in a cross correlation type of measurement. For the reconstruction of the temporal profile of a harmonic field E_q or a superposition of harmonic fields $\sum_q E_q$, the reference phase can be q-times the phase of a Fourier transform limited (FTL) fundamental laser field, q being the order of each harmonic of the superposition. This reference phase appears in ω_q vs $q\omega$ interaction schemes, like those utilized in the phase sensitive coherent control technique[25]. In this technique, the yield of the interaction of matter with a dichromatic field is controlled through the relative phases of the two phase-correlated waves, exploiting the degree of constructive or destructive interference governing the interaction. In an inverse manner, measuring the variation of an interaction yield, information about the relative phases of the interfering interaction channels can be extracted and thus field phase distributions may be retrieved.

It was recently proposed a cross correlation approach based on this principle, i.e., on ω_q vs. $q\omega$ ionization of atoms, that allows for the full spectral phase distribution retrieval of ultra-short harmonic pulses[26]. Here, the term "full" describes both the relative spectral phase between harmonics as well as between different frequency modes within the bandwidth of

each harmonic. A simplified "all optical" version of the approach, measuring a total harmonic generation yield instead of ionization has been successfully implemented in reconstructing the temporal profile of FTL as well as chirped third harmonic fields of a Ti:Sapphire laser produced in a gas medium[24]. In this modified version the "phase control" is not only through quantum interference control of the induced atomic polarization, but also through macroscopically controlled phase matching between the interfering fields. The generated harmonics co-propagate with the fundamental, entering a transmission grating Michelson interferometer described in detail elsewhere[27].

The interferometetric setup selects the 3rd and 5th harmonic from the entire harmonic spectrum. The high precision piezoelectric translation stage of the interferometer allows for the introduction of a variable delay (phase shift) between the fundamental and the two harmonic fields. The three fields, with frequencies ω, ω_3 and ω_5, are subsequently focused in a second Xe gas cell, which henceforth will be called the second non-linear medium (NLM-2). In NLM-2 the harmonics are generated by the fundamental in the presence of the harmonic fields produced in NLM-1. The coupling scheme in the NLM-2 is depicted in Figure 1.3-1.

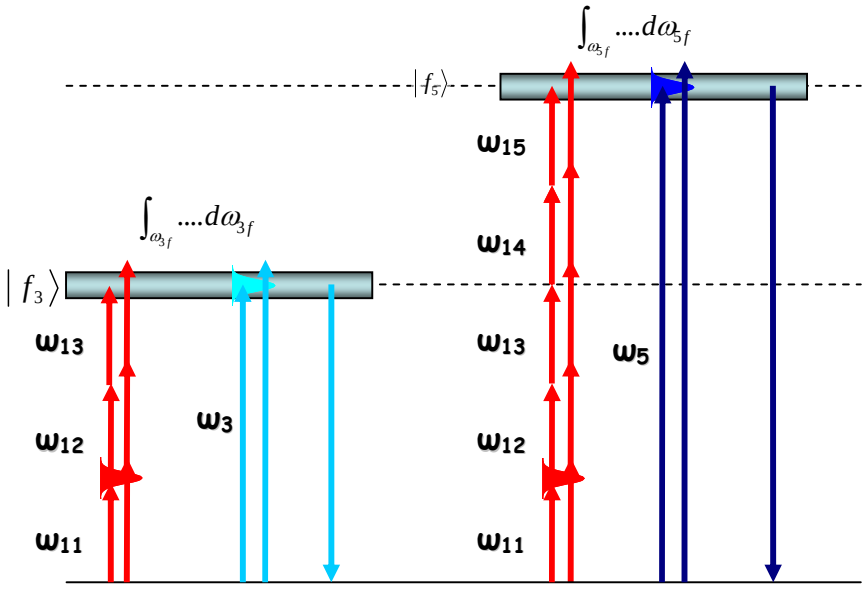

Figure 1.3-1: Scheme of the interfering channels leading to an excitation probability depending on the relative phase between the corresponding fundamental and the harmonic modes.

The superposed 3rd and 5th harmonic fields to be characterized are cross correlated with the FTL laser field in a three vs one and five vs one coupling scheme, respectively. In order for the fundamental laser pulse to be FTL in the NLM-2 a pre-compensated fundamental pulse has been used. As criterion for the presence of FTL fundamental pulses in the NLM-2, the maximization of the harmonic generation has been used by adjusting the chirp value of the fundamental pulse before entering the NLM-1.

In the following discussion it is assumed that all interactions are within the lowest order perturbation theory (LOPT) and that the fundamental field $E_{\omega}(\omega, z, t)$ is FTL. In the second non linear medium (NLM-2), the propagation equation for any of the harmonic frequency components ω_q (q=3, 5) within the spectral region of interest, results in a harmonic field at the exit of the NLM-2

$$E_{\omega_q}(z = L) = E_{\omega_q}(z = 0) + A\int_0^L P(\omega_q, z, t)dz\,, \tag{2.1}$$

where z=0 is the position of the entrance of the NLM-2, and thus $E_{\omega_q}(z = 0)$ is the harmonic field entering this medium, i.e., the field produced in the first non linear medium (NLM-1) modified through propagation. L is the length of NLM-2 and A is a constant. $P(\omega_q, z, t)$ is the polarization of the medium at ω_q, which in general consists of interfering non linear P^{NL} and linear P^{L} terms:

$$P(\omega_q, z, t) = P^{NL}(\omega_q, z, t) + P^{L}(\omega_q, z, t) = \chi^{(q)}E_{\omega}^{q}(z, t) + \chi^{(1)}E_{\omega_q}^{NLM1}(z, t)\,, \tag{2.2}$$

where $\chi^{(q)}$ and $\chi^{(1)}$ are the non linear and linear susceptibilities at ω_q, respectively. Due to the resulting three interfering terms in (2.1), the emitted intensity at ω_q is

$$I_{\omega_q} = C + B \times \cos(\varphi_q(\omega_q) - q\varphi_L) \tag{2.3}$$

with C and B being constants and φ_q, φ_L the phases of the harmonic and fundamental fields, respectively. Introducing a variable delay τ between the two fields the measured intensity becomes oscillatory with τ and carries information about φ_q:

$$I_{\omega_q}(\tau) = C + B \times \cos(\varphi_q(\omega_q) - \omega_q \tau) \tag{2.4}$$

Note that, in this "all optical" arrangement, even when the linear term in (2.2) becomes negligibly small, the measured signal carries the same phase information. This is not the case when the measured quantity is ionization in the NLM-2[26] instead of harmonic generation, for which the two terms in (2.2) have to be comparable in strength.

For a polychromatic field, as is the case in the present experiment, the measured total harmonic signal at the exit of NLM-2 is the incoherent sum of intensity contributions of the type of (2.4) from all the spectral components involved in the interaction, i.e.

$$I_{TOTAL}(\tau) \propto \sum_{q=3,5} \int_{\omega_q} B(\omega_q) \cos(\varphi_q(\omega_q) - \omega_q \tau) d\omega_q \tag{2.5}$$

The summation, although redundant, is introduced in order to denote that the harmonic field is spectrally localized around the third and fifth harmonic of the fundamental. A Fourier transform of the cross correlation signal of (2.5) will result in the entire spectral phase distribution for the two harmonics under investigation.

Chapter 3

Analysis of the optical arrangement

A numerical simulation of the experiment, utilizing a three-dimensional (3D) ray tracing code for the analysis of the optical arrangement employed has been performed.

3.1 3D ray-tracing analysis

For the 3D ray-tracing the 3D capabilities of the OPTICA® package of Mathematica® have been used.

The 3D ray-tracing code is of particular importance in analyzing this set-up, since it can account for the effects of the beam propagation through the grating and the reflection of the tilted mirrors on the dispersion and focusing characteristics. Furthermore, it assesses the geometric aberrations due to the optical elements of choice and the geometry used

The code of the Mathematica® that is fully simulating the experimental setup is presented at the appendices in the end of this thesis (see *Appendix D : Mathematica® code used to simulate the experiment*, *Appendix B : Optica® code for the 3D ray tracing os the experimental setup*). The parameters that had used for this simulation are presented at the in the Table below.

Parameters	Configuration
λ_L (nm)	800
λ_3 (nm)	266
λ_5 (nm)	160
$N_{Grating}$ (l/mm)	600
x_{SM1} (mm)	300
x_{SM2} (mm)	300-320[i]
R_{SM1} (mm)	300
R_{SM2} (mm)	300
R_{SM3} (mm)	300
θ_{SM3} (deg)	~ 2.5
x_{SM3}† (mm)	140

In Figure 3.1-2 is presented the result of the 3D ray tracing code.

[i] Here should be noted that the distance grating and spherical mirror SM2 is variable

The ray-tracing code resulted that the centers of the two beams on the spherical mirror SM2 had a spatial separation of 2 cm (**Figure 3.1-1**). Thus the 1 inch diameter mirror had to be replaced with a 2 inch one unprotected gold mirror, succeeding in this way the highest possible reflectivity at the FH wavelength.

The ray- tracing shows that we need the smallest possible height h[ii] in order to avoid the astigmatism at the focus in the NLM-2. Thus the new spherical mirror should be tilted by ≈2.5°

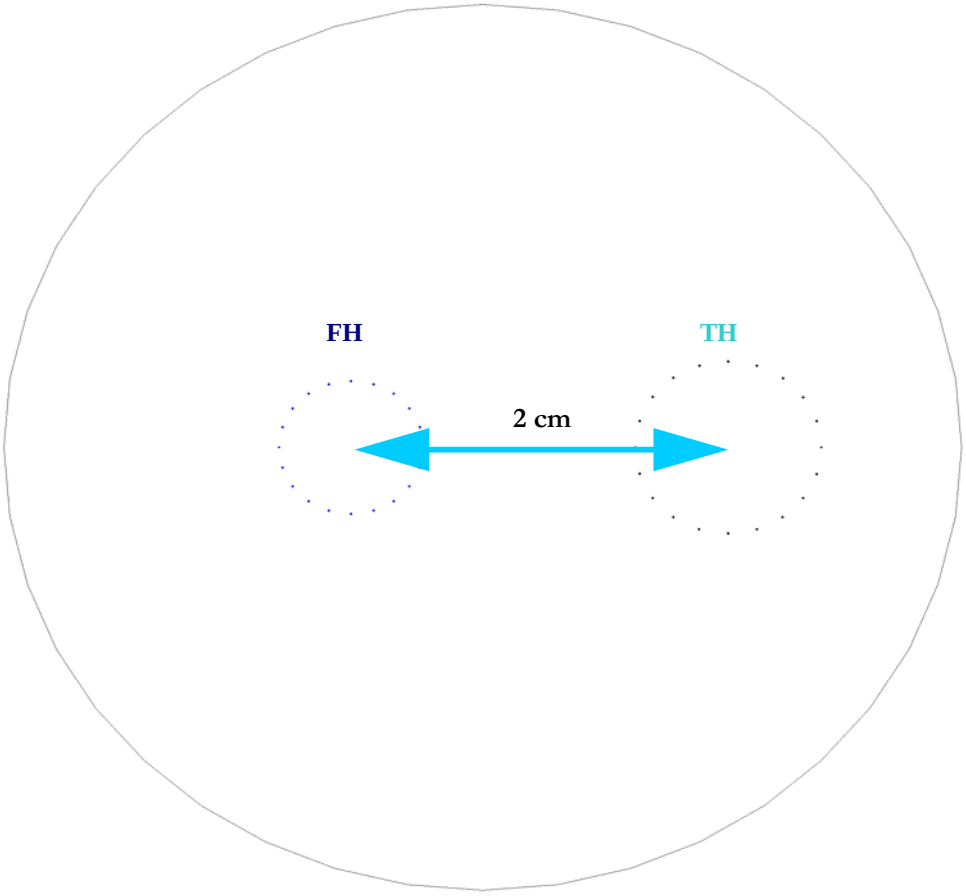

Figure 3.1-1: The result of the ray-tracing code that gives a spectral splitting of 2-cm between TH and FH on the mirror SM2**.**

[ii] Elevation height *h* is the height difference between the incoming beam and the retro-reflected beams on the grating.

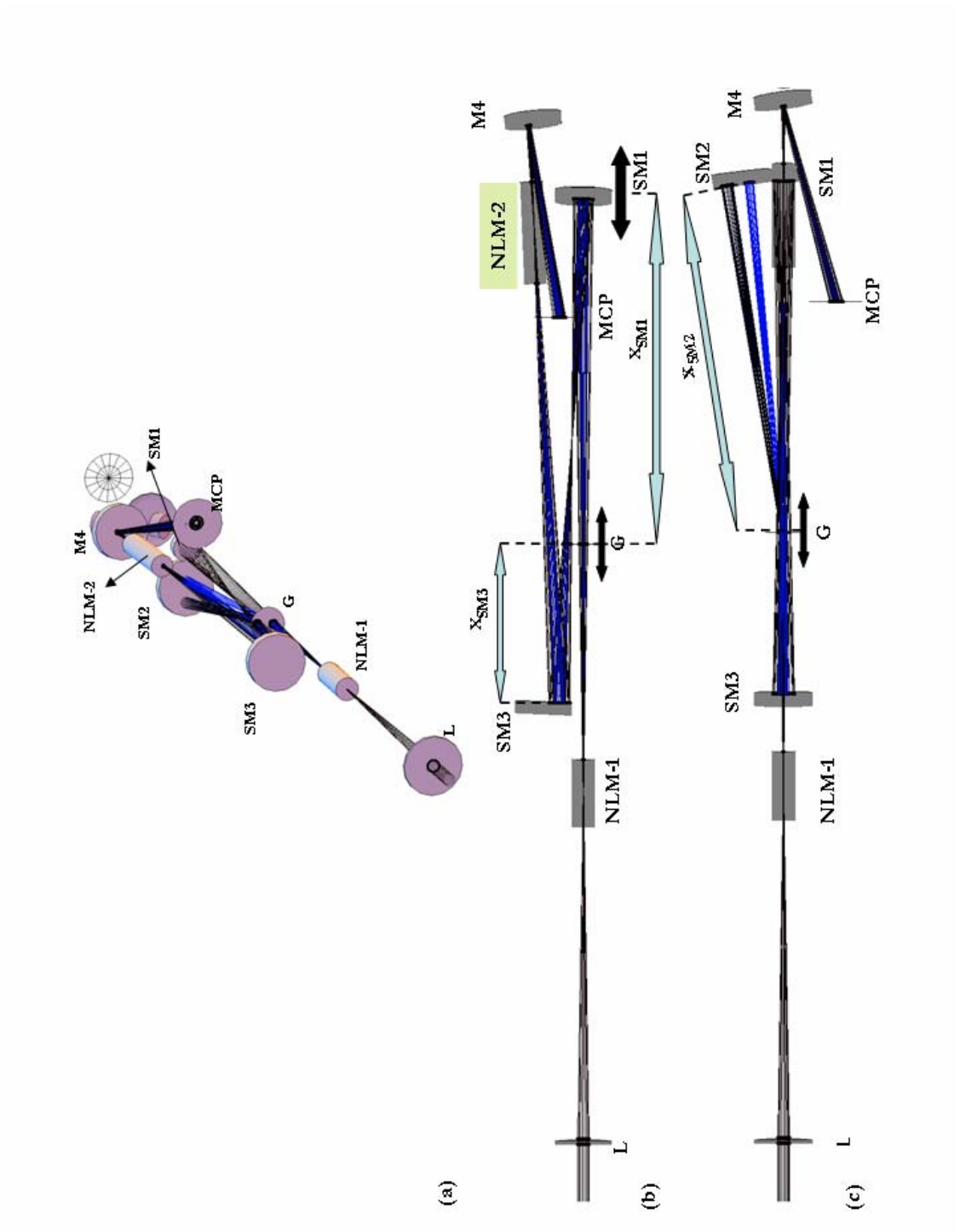

Figure 3.1-2: Schematic layout of the grating interferometer. *(a)* A full 3D view, (b) a side view and (c) a top view, as it was extracted from the optical ray-tracing.

CHAPTER 3

In the simulation, the propagation of the harmonic radiation through dispersive materials (1 mm thick Fused Silica (FS) transmission grating and 2 mm thick LiF entrance window in the NLM-2) has been taken into account.

An analytical code has been developed (see *Appendix D : Mathematica® code used to simulate the experiment*) in order to calculate the pulse duration of the harmonics and the group velocity dispersion (GVD) that was introduced. In order to calculate the refractive indices of the fused silica and the LiF we used the well known Sellmeier dispersion formula[28,iii]. The GVD factor D_2 is given by the equation (3.1)

$$D_2(\omega) = \frac{d}{c}\frac{\partial^2(\omega n(\omega))}{\partial \omega^2} \quad , \tag{3.1}$$

where d is the thickness of the material, c the speed of light in vacuum and ω the angular frequency of the radiation. For the TH and the FH the values for the D_2 are 391 fs^2 and 2499 fs^2 respectively.

The fundamental pulse had been negatively chirped in order to maximize the signal of the TH signal in NLM-2. This has been done in order to compensate the chirp introduced by the dispersive materials (1 mm fused silica grating (double pass), 3 mm thick BK7 glass (F) (double pass), 2 mm LiF window of NLM-2. According to the calculations the fundamental in the first cell should have FWHM duration τ_{fund}=70 ± 8 fs.

The harmonics start their propagation in the interferometric setup negatively chirped, pass through the 1 mm thick fused silica transmission grating (double pass which this means 2-mm) and the 2 mm thick LiF window of the NLM-2 before they were focused into it.

According to LOPT the duration of the q^{th} harmonic is given by $\tau_q = \tau_L / \sqrt{q}$, where q and τ_L are the harmonic order and the duration of the driving laser field, respectively. The

[iii] $n(\lambda)=\sqrt{\frac{A1\lambda^2}{\lambda^2 - B1^2} + \frac{A2\lambda^2}{\lambda^2 - B2^2} + \frac{A3\lambda^2}{\lambda^2 - B3^2} + 1}$,where Ai and Bi are constants and depend on the material.

FWHM durations of the TH and FH generated in the NLM-1, are $\tau_{TH}=\tau_{fund}/\sqrt{3}=40\pm 3$ fs and $\tau_{FH}=\tau_{fund}/\sqrt{5}=31\pm 3$ fs[iv], respectively and there are negatively chirped.

Using this result and considering that the harmonics propagate through 1 mm thick FS grating (double pass) and 2 mm thick LiF window, the non-linear chirp factors are found to be ~0 fs^2 (FTL) and ~2100 fs^2 for the TH and the FH, respectively.

Using the equation (3.2)

$$\Delta\tau=\frac{\tau_L}{\sqrt{n}}\sqrt{1+\left(4\ln 2\frac{D_2}{\frac{\tau_L}{\sqrt{n}}}\right)^2}\ , \tag{3.2}$$

(where $\tau_L=56$ fs, n is the order of harmonic and D_2 is the non-linear chirp factor) we can extract the FWHM durations of the TH and FH in the second cell NLM-2. The FWHM pulse durations should be 32 fs and 270 fs for the TH and the FH respectively.

The two harmonics have different optical paths due to FS grating. The optical path difference is given by the equation (3.3)

$$OPD=\frac{(n_1-n_2)2d}{c}\approx 800\,fs \tag{3.3}$$

In order to cancel out this optical path difference the grating is displaced. The Figure 3.1-3 depicts the optical path difference of the two harmonics vs. the distance of the grating from the SM2 (x_{SM2} in Figure 3.1-2) as it was extracted by the 3D ray-tracing code. Using as initial position SM2-grating (x_{SM2} in Figure 3.1-2) a distance of 300mm, the x-axis shows the distance difference from this value due to the displacement of the grating.

Using the results of these calculations we can compensate the OPD that is introduced by the FS grating by moving the grating ~10 mm away from its initial position. This is similar to the principle of a grating compressor in conventional laser systems

[iv] These values correspond to the intensity FWHM pulse durations

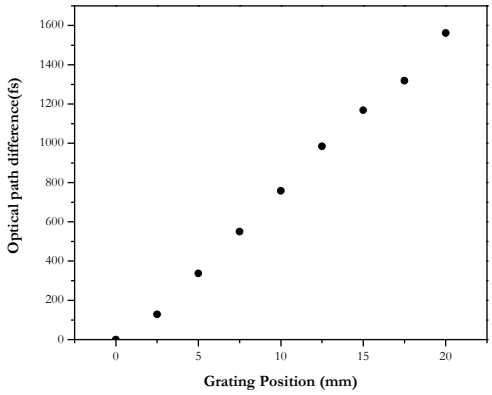

Figure 3.1-3: Optical Path Difference (OPD) with the displacement of the grating as it was extracted from the 3D ray-tracing code.

3.2 Numerical Evaluations

Using the equation(2.5) and the results of the 3D ray tracing code, the cross-correlation trace shown in Figure 3.2-1(a) has been simulated for a delay range from -25 fs to 25 fs. Propagation of the TH radiation is found to induce negligible chirp. The harmonic spectral amplitudes, shown in Figure 3.2-1 (b), (c), have been taken to be equal with their experimental values. From these spectral phase and amplitude distributions the simulated harmonic field superposition has been reconstructed. For the 56 fs long laser pulse, the FTL duration of the 3rd and 5th harmonic is expected to be 32 fs and 25 fs, respectively. The pulse duration of the reconstructed temporal profile is founded to be close to its FTL value (32 fs) for the 3rd harmonic pulse and 270 fs for the chirped 5th harmonic pulse. The temporal separation between the 3rd and 5th harmonic field which is introduced by the propagation of the fields in the dispersive materials is partially compensated in the experiment by changing the grating position in the interferometer. In the simulation, the temporal separation between the two harmonic pulses is arbitrarily set to 120 fs.

Figure 3.2-2 depicts the two reconstructed fields and the time delay between them as resulted from the Fourier synthesis (see *Appendix E: Mathematica® code used for the pulse reconstruction*)

$$F(t) = \sum_{j=1}^{N} S(\nu_j) \exp(i\phi(\nu_j)) \exp(i\, 2\pi\nu_j\, t), \tag{3.4}$$

using the above retrieved spectral amplitude $S(\nu_j)$ and spectral phase distribution $\phi(\nu_j)$. In eq.(3.4) N is the number of the sampling points. The pulse duration found for the TH by

fitting a Gaussian function on the reconstructed pulse is 32 fs[v]. The FH pulse duration is found to be 270 fs. The inset in the Figure 3.2-2 shows the interference structure of the superposed TH and FH field.

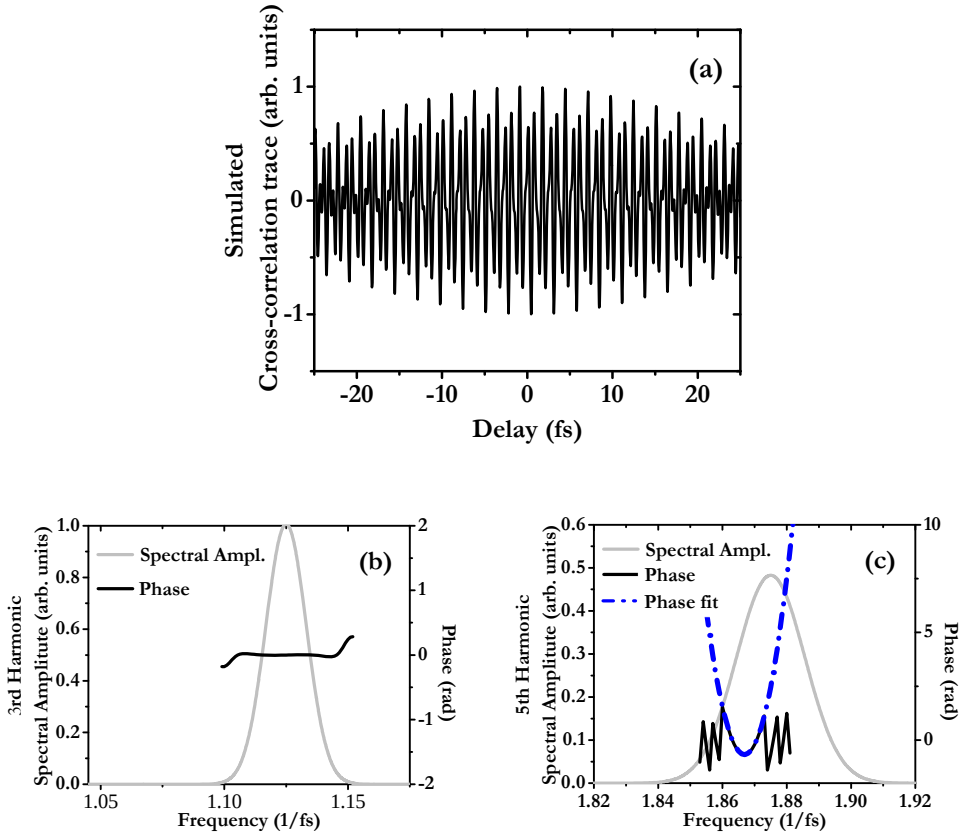

Figure 3.2-1: The simulated cross-correlation trace between the IR and the superposed 3rd and 5th harmonic field (a). Fourier transforms spectra (b) and (c). In (b) and (c): Extracted spectral phase distribution of the simulated superposed 3rd and 5th harmonic field (black line). Grey line: Spectral amplitudes of the 3rd and 5th harmonic

[v] These values correspond to the intensity FWHM pulse durations.

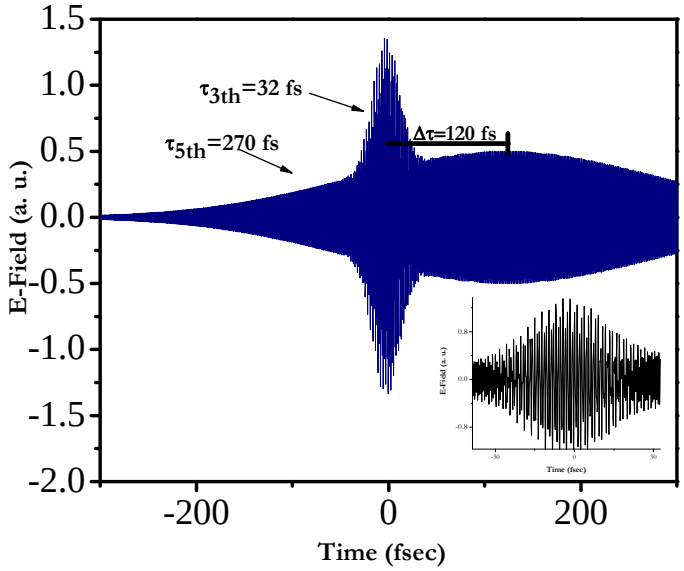

Figure 3.2-2: The reconstructed pulses are produced through Fourier-synthesis using the retrieved spectral phase from the simulated cross-correlation data of Figure 3.2-1 (a) and the spectral amplitude distribution of Figure 3.2-1 (b),(c) for the TH and FH, respectively. The time delay between them is 120 fs. The inset shows the interference structure of the superposed 3rd and 5th harmonic field.

3.2.1 Fourier Deconvolution

The analysis of real world signals is a fundamental problem for many engineers and scientists, especially for electrical engineers since almost every real world signal is changed into electrical signals by means of transducers, e.g., accelerometers in mechanical engineering, EEG electrodes and blood pressure probes in biomedical engineering, seismic transducers in Earth Sciences, antennas in electromagnetism, microphones in communication engineering, etc.

Traditional way of observing and analyzing signals is to view them in time domain. Baron Jean Baptiste Fourier[29], more than a century ago, showed that any waveform that exists in the real world can be represented by adding up sine waves. Since then, we have been able to build our real world time signal in terms of these sine waves. It is shown that the combination of sine waves is unique; any real world signal can be represented by only one combination of sine waves.

3.2.1.1 Windowing and Window Functions

Using a finite-length discrete signal in the time domain in FT calculations is equivalent appling a rectangular window to the infinite-length signal[30]. This does not cause a problem with the transient signals which are time-bounded[vi] inside this window. The problems appear when the processed signals are continuous, like a sine wave. If the length of the window contains an integral number of cycles of the time signal, then, periodicity introduced by discretization makes the windowed signal exactly same with the original. In this case, the time signal is said to be periodic in the time record. On the other hand, there is a difficulty if the time signal is not periodic in the time record, especially at the edges of the record (i.e., window). If the *Discrete Fourier Transform* (DFT) or *Fourier Transform* (FT) (see *Appendix A: Fourier transform* for details) could be made to ignore the ends and concentrate on the middle of the time record, it is expected to get much closer to the correct signal spectrum in the frequency domain. This may be achieved by a multiplication by a function that is zero at the ends of the time record and large in the middle. This is known as *windowing*.

It should be realized that, the time record is tempered and perfect results shouldn't be expected. For example, windowing increases spectral leakage[vii]. It should also be noted that, windowing is introduced to force the time record to be zero at the ends. Therefore transient signals which occur (starts and ends) inside this window do not require a window. They are called *self-windowed* signals, and examples are impulses, shock responses, noise bursts, sine bursts, etc.

In our case the recorded signal has a length of 270 fs. Due to the limitations that are inserted by the piezoelectric crystal, the recorded signal has a length of 50 fs (-25 fs to 25 fs). This means that the DFT of the windowed signal is the convolution of the h(t) (window function) and the real signal S(t) ($F(v) = h(v) \otimes S(v)$).

The Fourier transform of a window function is a real function

[vi] **Time-bounded** are called the signals that are smaller than the length of the window

[vii] **Spectral leakage** is an effect in the frequency analysis of signals where small amounts of signal energy are observed in frequency components that do not exist in the original waveform. The term 'leakage' refers to the fact that it appears as if some energy has 'leaked' out of the original signal spectrum into other frequencies

$$h(v) = \frac{Sin(a\,\pi v)}{a\,\pi v}, \tag{3.5}$$

where *a* is the length of the window.

This means that there is no introduction of new phases in the spectral phase distributions but there is a modificattion of the amplitude distribution. Figure 3.2-4 depicts the Fourier transform of the signal in Figure 3.2-1 using the FFT and DFT.

The TH harmonic spectrum isn't affected by the window function because the length of the window is bigger (50 fs) than its FWHM duration (32 fs). On the other hand there is a significant difference between the FFT and the DFT for the FH. First of all spectral leakage is observed and there is a small deviation from the central frequency due to the partial contribution of the FH to the DFT. The above reflects the conditions of our experimental data analysis.

As it was noted before the convolution with the window function doesn't affect the spectral phase distribution but is widened by the spectral leakage to the FWHM of the spectral amplitude distribution. In order to recover the "real" spectral phases we have to multiply the phases of the FH of the Figure 3.2-4(b) with the function $\frac{ph_{DFT}(v)}{ph_{FFT}(v)}$, where $ph_{DFT}(v)$ and $ph_{FFT}(v)$ are the spectral phase distributions of each case (Figure 3.2-3).[viii]

Here should be noted that this method is justified for our experimental data analysis but it's not a general correction method.

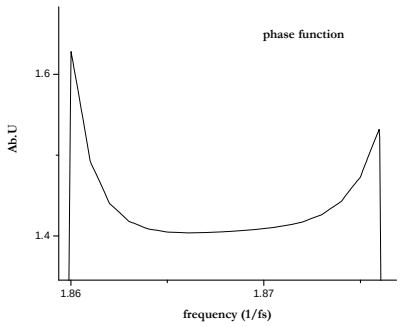

Figure 3.2-3: Phase Correction Function

[viii] Here should be noted for the phase correction function depends on the window function. The phase correction presented is only for realization purposes.

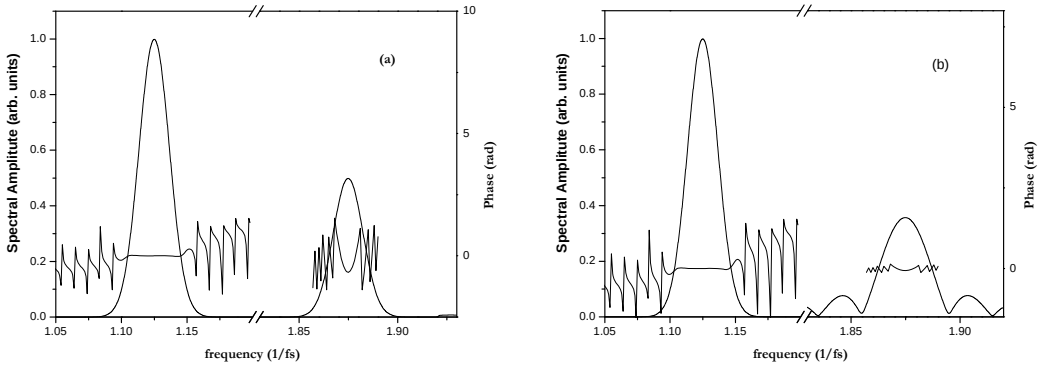

Figure 3.2-4: Fourier transform spectra of the signal of Figure 3.2-1 using the (a) FFT and (b) DFT approach.

Chapter 4

Experimental Part

4.1 The femtosecond Ti:Sapphire Laser system

All the experimental work of this thesis was carried out using the femtosecond Ti:Sapphire amplified laser system at the Ultraviolet Laser Facility (U.L.F.) of the I.E.S.L – F.O.R.T.H. A schematic layout of the complete laser system is depicted in

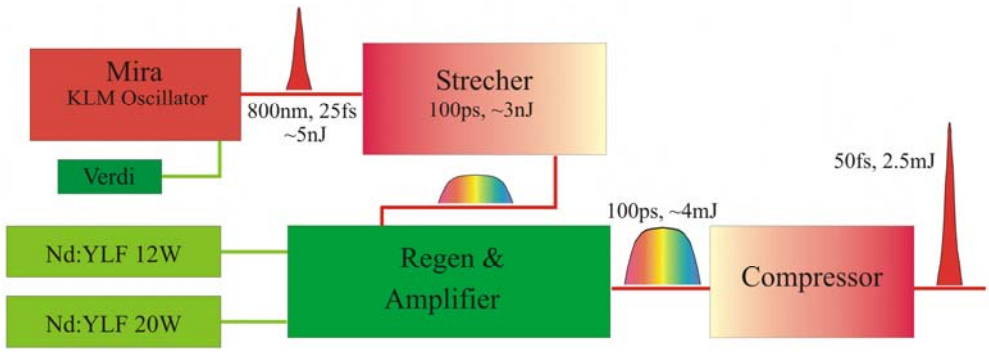

Figure 4.1-1: **A** schematic layout of the pulse amplification stages of the Ti:Sapphire laser system

It comprises of a commercial Mira and B.M. Industries laser system using a combination of a Mira master oscillator, a pulse stretcher, a 1 kHz two-stage amplification configuration and a pulse compressor.

The spectral and temporal profiles of the nearly Fourier-transform limited amplified laser pulse are shown in Figure 4.1-2. The profiles have been measured with a commercial SPIDER (Spectral Phase Interferometer for Direct Electric-field Reconstruction) apparatus available by APE. The temporal width of the pulse is measured to be 56 ± 4 fs having a carrier wavelength at 803-nm.

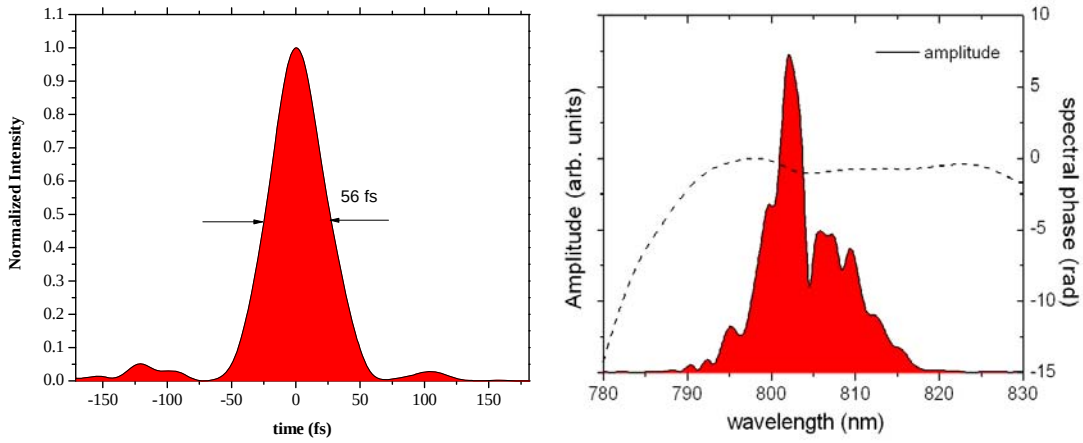

Figure 4.1-2: *Left:* The temporal and *Right* the spectral profile of the pulse from the amplified Ti:Sapphire laser system measured with a commercial SPIDER instrument available by APE. The dotted curve in the right figure represents the measured spectral phase. The almost flat spectral phase across the pulse indicates a nearly Fourier-limited pulse.

4.2 Optical layout

The experimental optical layout is depicted in Figure 4.2-1. The laser beam is focused by a 30-cm focal length planoconvex lens into a 30 cm long static cell filled with Xe in which harmonic generation takes place. A 0.3 mm diameter pinhole is placed at the exit of the gas-cell. The later is utilized for the separation of the gas-cell from the vacuum chamber. In addition, by focusing the beam slightly after the pinhole the THG signal was observed to be maximized. The fundamental and the generated at the gas cell harmonics enter into the vacuum chamber where the grating-interferometer is built in. The beams are spectrally dispersed by a 1 mm thick fused silica transmission grating of 600 lines/mm optimized for maximum throughput at 266 nm.

The zeroth-order of the fundamental pulse passes through a 3 mm thick BK7 glass (F) in order to filter out the zeroth-order harmonics and impinges on a 30 cm radius of curvature, 1 inch diameter gold unprotected spherical mirror (SM2) mounted on a piezoelectric crystal. The mirror-piezoelectric crystal system is mounted on a piezoelectrical translation stage for ruff displacement. The first-order of the spectrally dispersed TH and FH impinge a second 30 cm radius of curvature, 2 inch diameter gold unprotected spherical mirror (SM1). The diffraction angle has been calculated to be ~9.2^{o} for the TH and 5.5 ^{o} for the FH. Both

mirrors are tilted by ~ 2.5 ^{o} and the retro-reflected beams are sent back to the grating having an elevation height of ~8 mm[ix]. The zeroth-zeroth-order of the fundamental and the first-first-order of the TH and the FH are focused into a second 10 cm long (NLM-2) static cell by the third 30 cm radius of curvature, 2 inch of aperture gold unprotected spherical mirror (SM3). The mirror SM3 is located in a distance of 140 mm from the grating. NLM-2 is of cylindrical shape with a diameter of ~12 mm, it is filled with Xe gas and it is closed with 2 mm thick LiF windows. The resulting signal recorded by a MCP (Multi Channel Plate) detector using a fourth 2 inch of aperture gold unprotected mirror (M4). The M4 and MCP system is mounted on a one dimensional translation stage.

In order to image the interaction region in the NLM-2 and subsequently optimize the alignment, a mirror M4 is moved out of the beam axis, and the beam (consisting of the TH pulses as the FH pulses don't propagate in air) is guided outside the chamber through a thin (3 mm) fused silica glass window. Then a 2 m focal length lens is imaging the interaction region in a distance of ~3 m where the CCD is placed. The latter comprises an important fine alignment tool when the chamber is under vacuum. In addition, the spherical mirror SM1 is mounted on a two-dimensional (θ-φ) pico-motor control unit giving the possibility of being remotely controlled.

For the fine alignment procedure, when the chamber is under vacuum conditions, the two generated TH pulses are spatially overlapped outside the chamber (the FH doesn't propagate in air). This can be easily accomplished by looking far away the image of their focus and by fine adjusting their relative position using the pico-motorized mirror SM2. Their spatio-temporal interference can be achieved by finding the zero-delay of the two overlapping pulses. In addition, the observation of a single spatial interferometric fringe indicates the existence of two co-propagating and interfering pulses after their recombination at the grating. After this observation the system MCP-M4 is moved in order to send the beam to the MCP to record the interference signal.

Figure 4.2-2 depicts the single spatial interfering fringe obtained through co-propagation of both interfering pulses as recorded for different delays between the two pulses by the CCD camera at the exit of the vacuum chamber. In addition, they depict the significant role

[ix] Elevation height is the height difference between the incoming beam and the retro-reflected beams on the grating.

of the mirror SM3, which by proper use, eliminates the shifting of the spatial fringes at different delays due to the relative tilt of the pulse fronts.

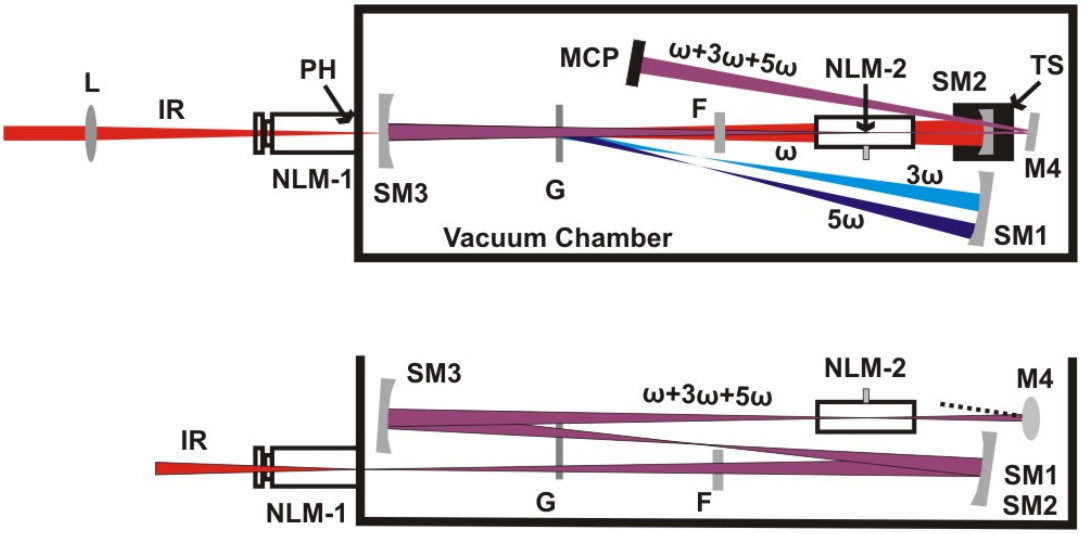

Figure 4.2-1: A schematic layout of the experimental set-up*: Top:* a top view and *bottom: a* side view. The fundamental beam from the Ti:Sapphire laser system is focused into the NLM-1 by a f = 30-cm lens L. The generated TH, FH and the fundamental enter into the vacuum chamber after passed though a pinhole PH and impinge onto the 600-lines/mm grating G. The spectrally dispersed first-order TH and FH are reflected back to the grating by the mirror SM1 slightly elevated in the vertical axis. The zeroth-order TH and FH are filtered out by a 1-mm-thick BK7 glass and thus only the fundamental beam is reflected back to the grating by the spherical mirror SM1. The SM2 is mounted on a translation stage TS. The fundamental, the TH and the FH are focused into the NLM-2 by the spherical mirror SM3. Then cross-correlation signal is reflected from the mirror M4 to the MCP.

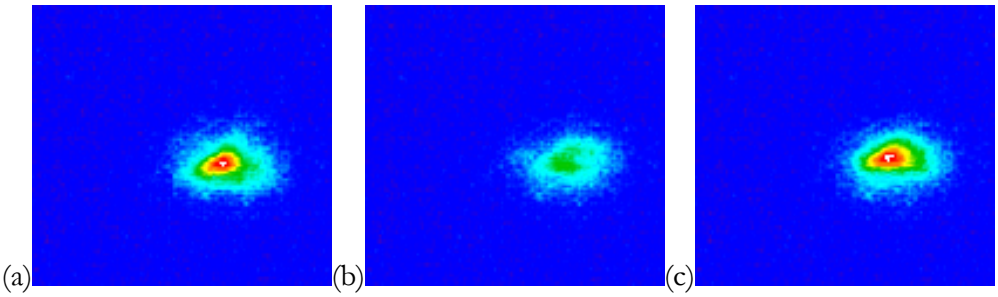

Figure 4.2-2: Spatial interference fringes of the TH recorded for three different delays between the two overlapping pulses. The images are captured by a CCD camera placed after mirror SM3 at the exit of the vacuum chamber. The mirror SM3 eliminates the shifting of the fringes due to the relative tilt of the pulse fronts

4.3 Vacuum Chamber

The experimental setup consists of a static cell (NLM-1) and a vacuum chamber. The quasi static cell is filled with Xe gas at laminar flow pressure (~50 mbar) where the production of the harmonics occurs. The cell is connected to the vacuum chamber through 0.3 mm aperture. The cylindrical chamber, that hosts the interferometric setup including the second static cell (NLM-2) and the MCP detector, has an internal diameter of 71cm and a height of 30 cm. NLM-2 was mounted on an aluminum platform avoiding contact with the interferometric setup in order to decouple the vibrations introduced by the rotary pump. The interferometric setup was built on a suspension mechanism to minimize the mechanical vibrations from the environment. The vacuum chamber was pumped by two turbomollecular pumps, having 150 l/s pumping speed each, joint in parallel and further pumped by a rotary pump. Typical chamber pressures during the experiments were in the range of 10^{-5} - 10^{-4} mbar.

(a) 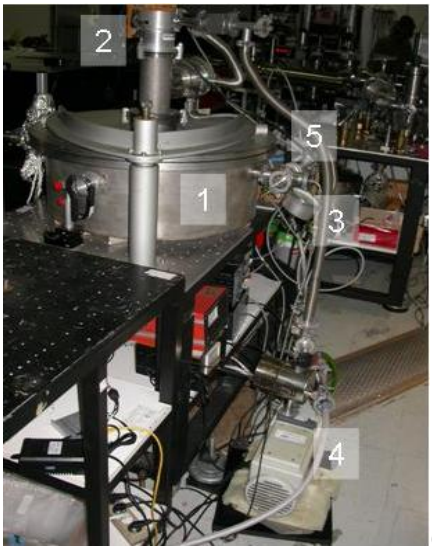

(b) 

Figure 4.3-1: (a) the vacuum chamber and the vacuum pumping system used. 1: Vacuum chamber. 2: Alcatel turbo pumps. 3: Pressure gauge for the generation cell. 4: Rotary pump, 5: Pressure gauge for the detection cell. (b) The interior of the vacuum chamber. 6: the MCP detector holder, 7: Alluminium platform which NLM-2 cell stands on

4.4 Data acquisition

Since the FH and higher harmonics don't propagate in air the signal had to be recorded in the vacuum chamber. Thus automation of the translation stage synchronization with the data acquisition was required. For this purpose computer software (see *Appendix G: Data acquisition Software*) was developed that synchronizes the oscilloscope, which records the signal from the MCP detector, and the piezoelectric crystal where the mirror SM2 is mounted on. In the next sessions we present the data acquisition system that was developed.

In this section is presented the electronic layout for the data acquisition. The figure depicts the electronic setup that it was built for these propose.

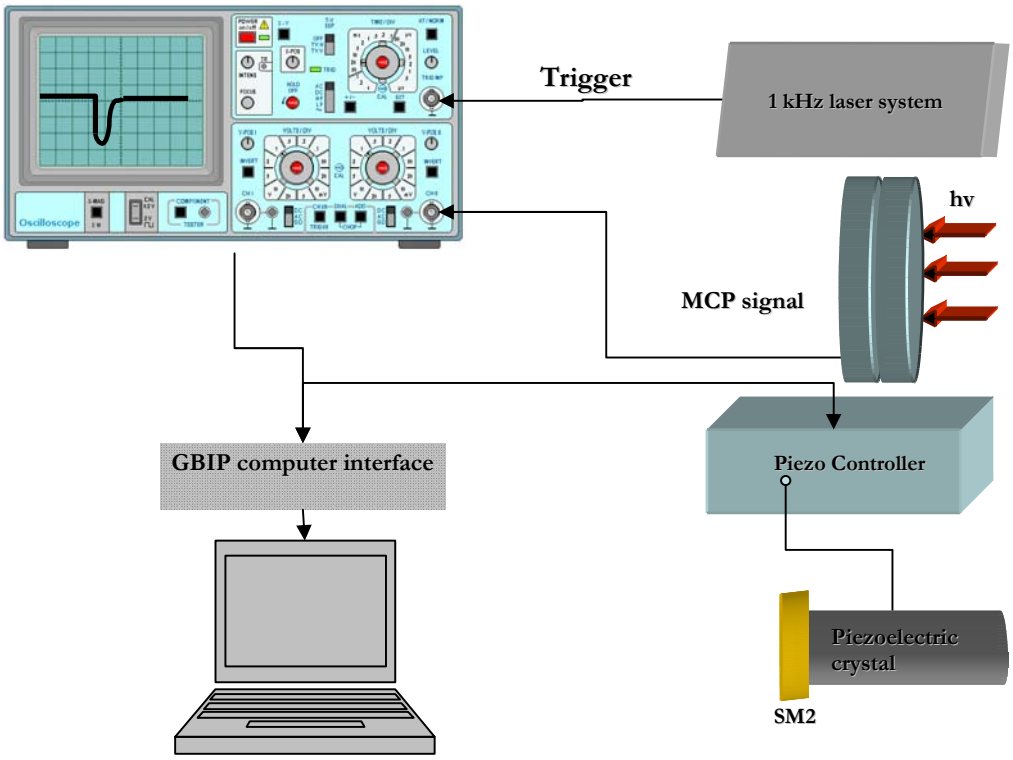

Figure 4.4-1: The electronic setup for the data acquisition.

The digital oscilloscope is triggered by the 1 kHz repetition rate of the laser. The oscilloscope is connected to the PC via GPIB interface. The oscilloscope averages the signal traces that are given by the MCP detector (for the selected by the user number of pulses) and sends the averaged signals to the PC for recording. After the recording the PC sends a command to the piezo-controller to drive the piezoelectric crystal to the next position. The

Piezo-Controller and PC system is connected via GPIB interface. This procedure is repeated iteratively until the piezoelectric crystal finds the desired position.

4.4.1 Micro- Channel Plate Detector (MCP)

MCPs are made up of a dense stack of millions of individual electron multiplier tubes, each tube having a diameter of typically 10 micrometer and a length of about 1 mm The distance between the tubes is only a little bit bigger than the tube diameter. Macroscopically, MCP are thin discs of a few centimeter diameter having typically 1 mm thickness. Under a microscope the microstructure reveals and the tiny and densely packed pores that are the entrances to the individual tubes become visible. The "open area ratio", i.e. the ratio of integrated pore area to the total disc area is usually at least 50%. While the front and back surface of an MCP is coated with metal (input and output electrode), the inside of the tubes is covered with a semi-conducting layer that tends to emit secondary electrons under the bombardment of primary energetic particles, such as photons (UV and higher) or charged particles as electrons. By biasing the MCP electrodes with a high electric field (about 1000 V/mm), each of the secondary electrons gains enough kinetic energy to liberate more electrons when it hits the wall. As in every other type of electron multiplier, an avalanche of electrons is forming along the tube that has a charge of a few thousands to a million e (depending on L/D and the electric field), finally exiting the pore. What makes the MCP unique is the localization of the charge cloud into one tiny pore and the presence of a vast number of pores over a larger area that operate independently.

Figure 4.4-2 presents the electronic layout of the MCP detector that was used in the experiment. The MCP detector is biased through a voltage divider consisting of a resistor R1 (1.8 MΩ) and a resistor R3 (10 MΩ) that is connected in series with the R2 (0.18 MΩ) in order to minimize the current that passes to the capacitor C (200 pF). The capacitance of C was selected in such a way that the discharging time will be some hundreds of psec. The operational voltage range of the detector was between 2.3-2.7 kV.

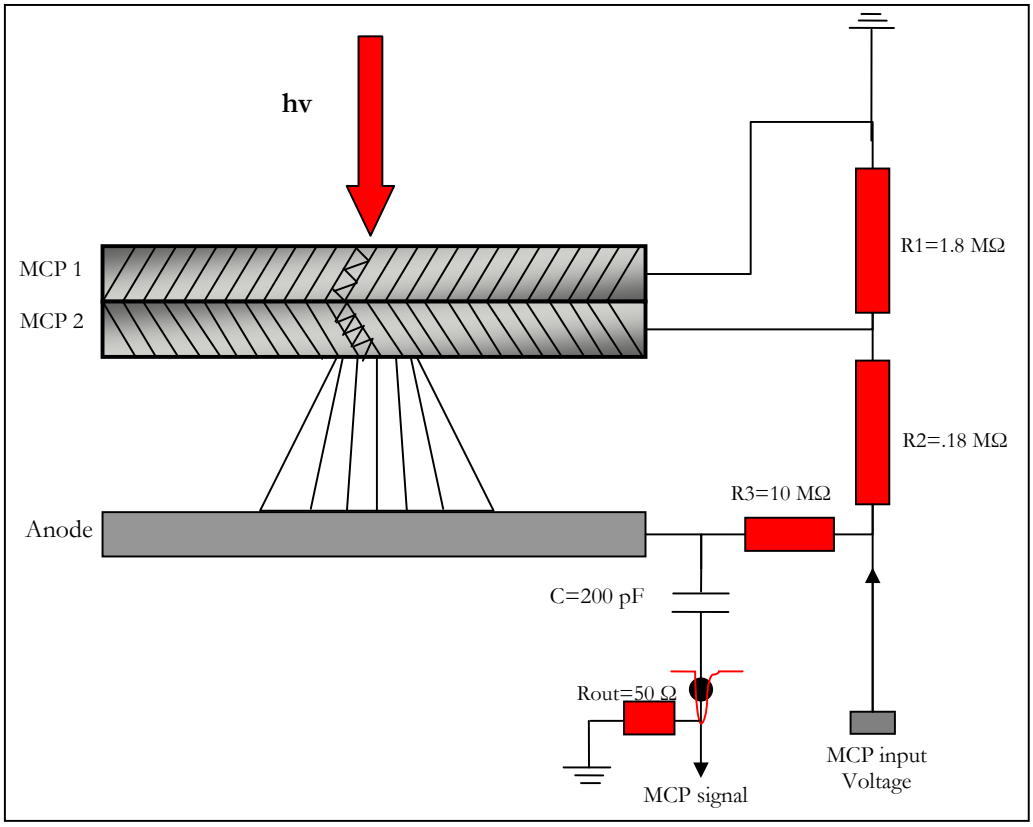

Figure 4.4-2: The electronic layout of the MCP.

4.4.2 Stepper-Motor resolution test

Piezoelectric crystals are designed to operate with high linearity in micrometer or sub-micrometer scale. Our piezoelectric crystal had a step-size of some nanometers. In order to check the resolution of the device and to test its linearity in this resolution range the field auto-correlation signal of the TH (267 nm) was recorded. It should be noted that this test includes also the performance of the built-in software acquisition, and the computer in use.

Figure 4.4-3 show the observed signal using the resolution option of 5 nm/step (PC value). The resolution is expected to be 10 nm (i.e. ~27 points per optical cycle) that it is found in agreement with the experimental result (10.16. nm i.e. ~28 points per optical cycle). Note that the resolution of the stepper-motor is the half of this value due to retro-reflection of the beam from the spherical mirror that is mounted on it. All the experimental measurements have been carried out by using the resolution used in the recording of Figure 4.4-3.

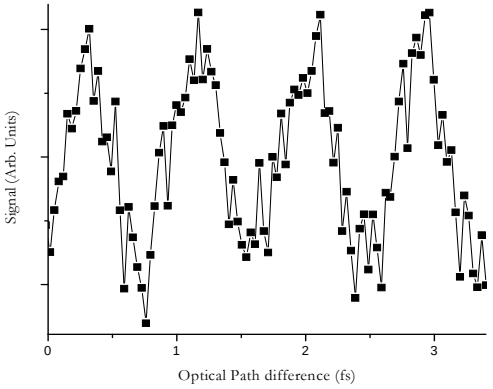

Figure 4.4-3: Stepper-motor resolution test performed through field autocorrelation measurements of the TH (267 nm). Figure depicts an expended area of the field autocorrelation between 0-3.5 fs.

4.4.3 Stability of the experimental set-up

Maximization of the temporal resolution requires stable experimental conditions. Vibration originality from mechanical and environmental sources affects the stability of interferometric set-ups. Mechanical vibrations originate from the translating mechanical parts of the set-up, e.g. the piezoelectric translation stage, the vacuum pumping system, as well as the surrounding environment.

In order to overcome such disturbances we performed passive isolation methods. An anti-vibration mechanism was constructed. This mechanism consists of three bronze columns placed symmetrically around the center of the optical table. The table is hanged by rubber belts thus remaining pendulous inside the vacuum chamber. In addition, a damping ring was placed between the turbo pumps and the chamber. Moreover all the optical elements in the vacuum chamber were mounted on thick heavy mounts. The above measurements seemed adequate to isolate the interferometric setup and allow for a high resolution recording of the traces.

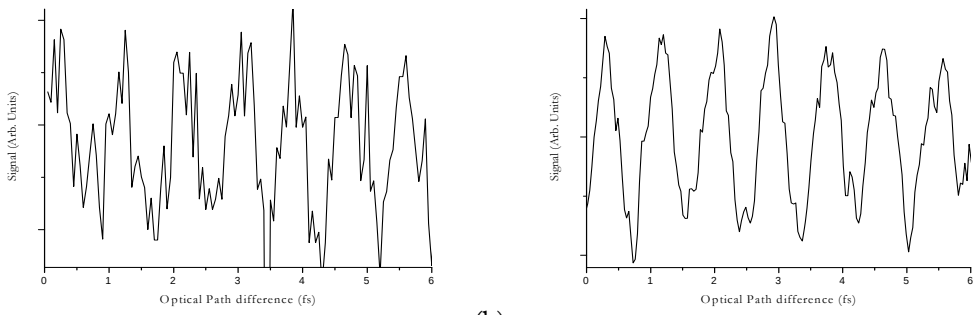

. (a) (b)

Figure 4.4-4: Autocorrelation measurements of the TH in the case where the interferometer, (a) is not isolated from mechanical noise sources (the experiment performed in air) and (b) when is isolated.

Chapter 5

Results and discussion

5.1 Cross-correlation measurements

The fundamental pulse with energy 1 mJ is focused into the first gas-cell filled with 50-mbars of Xe and its FWHM duration is τ_{fund}=70 ± 8 fs. The pulse had been negatively chirped to maximize the signal of the TH signal in the second gas-cell (NLM-2). This has been done in order to compensate the chirp that was introduced by the optical glasses before focused into the NLM-2.

The harmonics enter the interferometric setup having negative chirp, pass through the 1 mm thick fused silica transmission grating (double pass which this means 2-mm) and through a 2-mm-thick LiF window of the NLM-2 before they are focused into it. The signal of the fundamental is maximized in the NLM-2. This means that the positive dispersion that is introduced by the dispersive materials and the negative dispersion from the compressor canceled out. Thus, the fundamental in the NLM-2 is Fourier Transform Limited (FTL) with FWHM duration of 56 fs.

The TH and FH are differently dispersed through the propagation. The generated TH and FH pulses are negatively chirped at their generation in the first cell. The positive chirp that is introduced by the optical glasses increases their FWHM duration.

Figure 5.1-1 (a) shows the measured in the NLM-2 cross-correlation trace obtained by delaying the fundamental with respect to the generated in the NLM-1 FH and TH pulses. The average value of 100 samples per step was used. The inset in (a) depicts an expanded area of the cross-correlation trace showing the modulation of the signal in more detail.

In order to retrieve the spectral phase from the cross-correlation trace we used the expression φ(v) =-ArcTan[Im(A(v))/Re(A(v))] where $A(v)$ is the extracted complex spectral amplitude from the Fourier-transform (see *Appendix C : Mathematica® code used to extract the spectral phase and spectral amplitude.*). The black lines show the retrieved spectral phase

across the third and fifth harmonic peaks. Note that all the spectra recorded under these conditions showed a reproducible spectral phase distribution across the harmonic peaks.

In order to retrieve the spectral amplitude of the TH and the FH pulses a field autocorrelation measurement, was performed. For this purpose spatial interference of the recombined diffracted zeroth-first-order and the diffracted first-zeroth-order of the TH and FH pulses, by properly positioning the mirror SM3, was recorded. The harmonic generation conditions were the same as in the case of the cross-correlation. Figure 5.1-1 (b) and (c) (grey line) show the Fourier-transform spectrum of the field autocorrelation (a) for the TH and the FH, respectively.

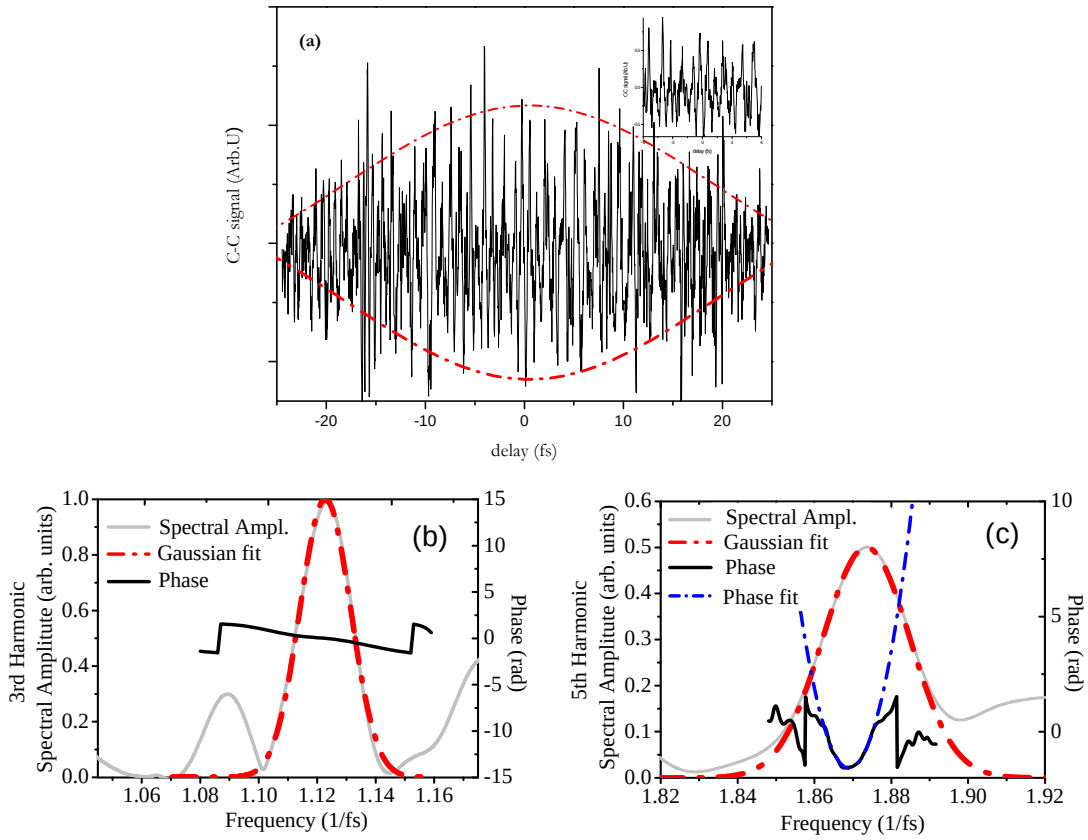

Figure 5.1-1: (a) Cross-correlation trace obtained by scanning the fundamental pulse across the TH and the FH pulses that are generated in the NLM-1. The red line depicts the Gaussian envelope fit to the cross-correlation trace. (b),(c) The black line depicts the retrieved spectral phase across the Fourier-transform spectrum of the cross-correlation trace. The grey line depicts the retrieved spectral amplitude across the Fourier-transform spectrum of the field autocorrelation for the TH and FH, respectively.

The field autocorrelation trace oscillates with two basic frequencies, the TH frequency (~1.123 fs^{-1}) and the FH frequency (~1.873 fs^{-1}). The cross-correlation trace, in this particular case, oscillates with two basic frequencies, the TH frequency (~1.123 fs^{-1}) and the FH frequency (~1.868 fs^{-1}).

This small deviation (for the FH) can be explained by the time delay between the two pulses. The Fourier transform of the cross-correlation trace gives the spectral phase distribution that corresponds to the frequency range of the FH pulse that contributes to the cross correlation signal (and not all the spectral bandwidth) due to the experimental limitations that introduces the piezoelectric crystal. This fact doesn't affect the result of the pulse reconstruction because the factor a^x of the non-linear chirp remains constant. In addition the variation from the central frequency of the field autocorrelation gives the time delay between the two pulses.

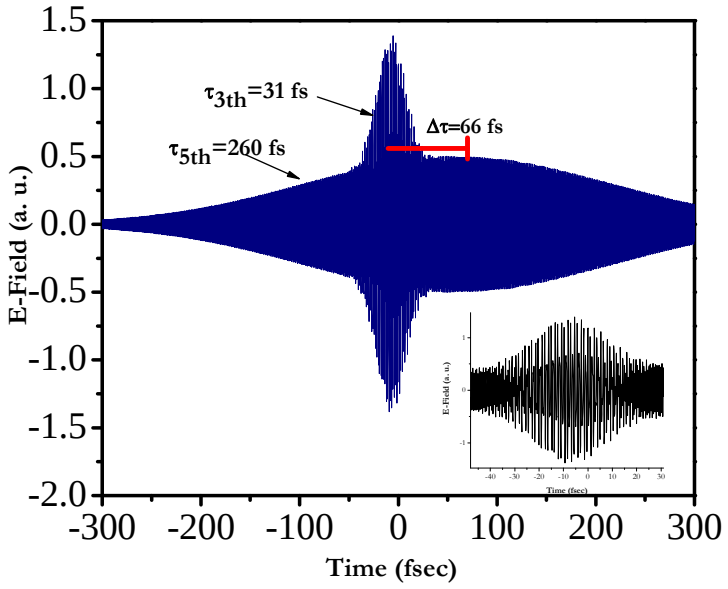

Figure 5.1-2: The reconstructed pulses are through Fourier-synthesis using the retrieved spectral phase distribution of the cross-correlation data of Figure 5.1-1 (b),(c) and the spectral amplitude distribution of Figure 5.1-1 (b),(c) for the TH and FH, respectively. The time delay between them is 66 fs. The inset depicts the interference structure of the superposed 3rd and 5th harmonic field.

[x] The phase distribution of a non-linear chirped pulse is in the form $\varphi(v)=\varphi_o+a\ v^2$ where a is the non-linear chirp factor

Figure 5.1-2 depicts the reconstructed TH and FH fields and the interference structure of them. The pulse duration found for the TH by fitting a Gaussian function on the reconstructed pulse is 31 ± 4 fs. The pulse duration of the FH found to be 260 ± 60 fs [xi]. The time delay between the two fields is found to be 66 fs due to a not complete compensation through the displacement of the grating. The low contrast of the beating is due to the significantly different amplitudes of the TH and FH. This result indicates that the approach is not restricted to fields with almost equal intensities.

5.2 Conclusion and Future Aspects

Concluding, the full spectral phase and amplitude distribution of an arbitrary superposition of the third and fifth harmonic fields of an 800 nm central wavelength, fs laser radiation, has been measured through a cross-correlation approach. Using the measured spectral phase/amplitude distributions the temporal profile of the superposed harmonic field has been reconstructed and found in agreement with simulations. The results reveal the suitability of the approach for full temporal characterization of broad band short wavelength radiation, such as high order harmonic superposition and thus of attosecond pulses and pulse trains. The technique is rigorously applicable, as long as harmonic generation in the NLM-2 is according to LOPT. This sets an upper limit to the order of the harmonics that can be characterized. Using He as NLM-2, phases of fields including harmonics up to the 15th of the 800nm laser radiation can be retrieved. Utilizing Xe as NLM-1 "plateau" XUV radiation with a bandwidth of ~10eV can be treated and thus attosecond pulses as short as 200 asec can fully reconstructed. For the characterization of waves with wavelengths below the LiF limit a free standing transmission grating has to be used [31] and the cells which contain the NLM should be replaced with gas-jets.

.

[xi] These values correspond to the intensity FWHM pulse durations.

Appendices

Appendix A: Fourier transform

The transformation from the time domain to the frequency domain (and back again) is based on the Fourier transform and its inverse, which are defined as

$$S(\omega) = \int_{-\infty}^{\infty} s(t) e^{-j2\pi\nu t} dt \tag{0.1}$$

$$s(t) = \int_{-\infty}^{\infty} S(f) e^{j2\pi\nu t} df \tag{0.2}$$

Here, *s(t), S(ω), and ν* are the time signal, the frequency signal and the frequency, respectively, and $j = \sqrt{-1}$. The physicists and engineers sometimes prefer to write the transform in terms of angular frequency $\omega = 2\pi f$, *as*

$$S(\omega) = \int_{-\infty}^{\infty} s(t) e^{-j\omega t} dt \tag{0.3}$$

$$s(t) = \frac{1}{2\pi} \int_{-\infty}^{\infty} S(\omega) e^{j\omega t} d\omega \tag{0.4}$$

which, however, destroys the symmetry. To restore the symmetry of the transforms, the convention

$$S(\omega) = \frac{1}{\sqrt{2\pi}} \int_{-\infty}^{\infty} s(t) e^{-j\omega t} dt \tag{0.5}$$

$$s(t) = \frac{1}{\sqrt{2\pi}} \int_{-\infty}^{\infty} S(\omega) e^{j\omega t} d\omega \tag{0.6}$$

is sometimes used. The FT is valid for real or complex signals, and, in general, is a complex function of ω (or *ν*).

The FT is valid for both periodic and non-periodic time signals that satisfy certain minimum conditions. Almost all real world signals easily satisfy these requirements (It should be noted that the Fourier series is a special case of the FT). Mathematically,

- FT is defined for continuous time signals.

- In order to do frequency analysis, the time signal must be observed infinitely.
-

. Discrete Fourier transform (DFT)

To compute the Fourier transform numerically on a computer, discretization plus numerical integration are required. This is an approximation of the true (i.e., mathematical), analytically-defined FT in a synthetic (digital) environment, and is called discrete Fourier transformation (DFT). There are three difficulties with the numerical computation of the FT:

- *Discretization* (introduces periodicity in both the time and the frequency domains)
- *Numerical integration* (introduces numerical error, approximation)
- *Finite time duration* (introduces maximum frequency and resolution limitations)

The DFT of a continuous time signal sampled over the period of T, with a sampling rate of Δt can be given as

$$S(m\Delta f) = \frac{T}{N} \sum_{n=0}^{N-1} s(n\Delta t) e^{-j2\pi m\Delta f\, n\Delta t} \qquad (0.7)$$

where $\Delta f = 1/T$, and, is valid at frequencies up to $f_{max} = 1/(2\Delta t)$.

As stated above, performing FT in a discrete environment introduces artificial effects. These are called aliasing effects, spectral leakage and scalloping loss. It should be kept in mind when dealing with discrete FT that:

- Multiplication in the time domain corresponds to a convolution in the frequency domain.
- The FT of an impulse train in the time domain is also an impulse train in the frequency domain with the frequency samples separated by $T_0 = 1/f_0$.
- The narrower the distance between impulses (T_0) in the time domain the wider the distance between impulses (f_0) in the frequency domain (and vice versa).
- The sampling rate must be greater than twice the highest frequency of the time record, i.e., $\Delta t \geq 1/(2 f_{\max})$ (Nyquist sampling criterion).

- Since *time – bandwidth* product is constant, narrow transients in the time domain possess wide bandwidths in the frequency domain.
- In the limit, the frequency spectrum of an impulse is constant and covers the whole frequency domain (that's why an impulse response of a system is enough to find out the response of any arbitrary input).

Appendix B: Optica® code for the 3D ray tracing os the experimental setup

This is the Optica® code for the ray tracing of the experimental setup

Experimental Setup - 3D Ray Tracing

```
Needs["Optica`Optica`"];

system2 = {
  Move[ConeOfRays[1.8/√3, NumberOfRays → 20,
    WaveLength → .8/3, Resonate → True, RayPointSize → 5.], {-230, 0, 0}],
  Move[ConeOfRays[1.8/√5, NumberOfRays → 20, WaveLength → .8/5,
    Resonate → True, RayPointSize → 5.], {-230, 0, 0}],
  (*Move[ConeOfRays[1.8/√7,NumberOfRays→20,WaveLength→.8/7,
     Resonate→True,RayPointSize→5.],{-230,0,0}],*)
  Move3D[Window[20, 60, EdgeRendering → Fill, ComponentMedium → Vacuum, Reflectance → 0.,
    GraphicDesign → Solid], {-250, 0, 0}, {Cos[-0π/180], Sin[-0π/180], Sin[0π/180]}, 0],
  Move3D[GratingSurface[600, 30, DiffractedOrders → {{1, 1.}}, GraphicDesign → Solid],
   {0, 0., 5}, {Cos[0π/180], Sin[0π/180], Sin[0π/180]}, 0],
  Move3D[SphericalMirror[305, 50, 10, Reflectance → 100.,
    EdgeRendering → Fill, GraphicDesign → Solid, GraphicDesign → Solid],
   {305 Cos[6.8π/180], 305 Sin[6.8π/180], 0}, {Cos[6.8π/180], Sin[6.8π/180], Sin[-1.35π/180]}, 0],
  (*Move[Screen[40,GraphicDesign→Wire],{90  Cos[5.5π/180],90  Sin[5.5π/180],5.5}],*)
  Move3D[GratingSurface[600, 30, DiffractedOrders → {{1, 1.}}, GraphicDesign → Solid],
   {0, 0., 5}, {Cos[0π/180], Sin[0π/180], Sin[0π/180]}, 0],
  Move[CircleOfRays[10, NumberOfRays → 20, WaveLength → .8,
    Resonate → True, RayPointSize → 5.], {-580, 0, 0}],
  Move[PlanoConvexLens[300, 50, 5, CurvatureDirection → Back,
    GraphicDesign -> Solid], {-530, 0, -0}],
  Move3D[GratingSurface[600, 30, DiffractedOrders → {{0, 1.}}, GraphicDesign → Solid],
   {0, 0., 5}, {Cos[0π/180], Sin[0π/180], Sin[0π/180]}, 0],
  Move3D[SphericalMirror[305, 26, 10, Reflectance → 100., EdgeRendering → Fill,
    GraphicDesign → Solid], {305 , 0 , 0}, {Cos[0π/180], Sin[0π/180], Sin[-1.35π/180]}, 0],
  Move3D[GratingSurface[600, 30, DiffractedOrders → {{0, 1}}, GraphicDesign → Solid],
   {0, 0., 5}, {Cos[0π/180], Sin[0π/180], Sin[0π/180]}, 0],
  (*Move[Screen[40,GraphicDesign→Wire],{-50,0,0}],*)
  Move3D[SphericalMirror[300, 50, 10, Reflectance → 100., EdgeRendering → Fill,
    GraphicDesign → Solid], {-140, 0, 35}, {Cos[-180π/180], Sin[-0π/180], Sin[2.5π/180]}, 0],
  Move3D[Window[20, 90, EdgeRendering → Fill, ComponentMedium → Vacuum, Reflectance → 0.,
```

APPENDICES

```
    GraphicDesign → Solid], {230, 0, 42}, {Cos[-0π/180], Sin[-0π/180], Sin[2.5π/180]}, 0],
  Move3D[Mirror[50, 10, Reflectance → 100., EdgeRendering → Fill, GraphicDesign → Solid],
   {370, 0, 44}, {Cos[7.5π/180], Sin[7.5π/180], Sin[6π/180]}, 0],
  Move3D[PinHole[45, 0, GraphicDesign → Solid], {200, -45, 20},
   {Cos[-0π/180], Sin[-0π/180], Sin[-0π/180]}, 0],
  (*Move3D[Screen[2,GraphicDesign→Wire],{260,0,42},
    {Cos[-0π/180], Sin[-0π/180],Sin[0π/180]},0],
   Move3D[Screen[2,GraphicDesign→Wire],{265,0,42},
    {Cos[-0π/180], Sin[-0π/180],Sin[0π/180]},0],
   Move3D[Screen[2,GraphicDesign→Wire],{273,0,43},
    {Cos[-0π/180], Sin[-0π/180],Sin[0π/180]},0],
   Move3D[Screen[2,GraphicDesign→Wire],{281,0,43},
    {Cos[-0π/180], Sin[-0π/180],Sin[0π/180]},0],
   Move3D[Screen[2,GraphicDesign→Wire],{288,0,43},
    {Cos[-0π/180], Sin[-0π/180],Sin[0π/180]},0],Move3D[Screen[2,GraphicDesign→Wire],
    {296,0,43},{Cos[-0π/180], Sin[-0π/180],Sin[0π/180]},0],*)
  Move3D[Mirror[22, 10, Reflectance → 100., EdgeRendering → Fill, GraphicDesign → Solid],
   {400, 0, 51}, {Cos[-0π/180], Sin[-0π/180], Sin[80π/180]}, 0],
  Move3D[Mirror[22, 10, Reflectance → 100., EdgeRendering → Fill, GraphicDesign → Solid],
   {400, 0, 6}, { -Cos[-0π/180], Sin[-0π/180], Sin[-113π/180]}, 0],
  Move3D[PlanoConvexLens[90, 50, 5, CurvatureDirection → Back, GraphicDesign -> Solid],
   {420, 0, 6}, {Cos[-0π/180], Sin[-0π/180], Sin[0π/180]}, 0],
  Move3D[Screen[45, GraphicDesign → Wire], {600, 0, 0},
   {Cos[-0π/180], Sin[-0π/180], Sin[-0π/180]}, 0],

  Boundary[300]
 };

da = PropagateSystem[system2];

a = DrawSystem[da, Boxed → False, PlotPoints → 10, QuickTrace → True,
    ThresholdIntensity → .2, RayLineThickness → .8, PlotType → Full3D,
    ViewPoint -> {-8.480, -1.925, 2.280}, OutputType → StandardGraphics];
```

Appendix C: Mathematica® code used to extract the spectral phase and spectral amplitude.

Data Processing Code

```
DataTable = Import["D:\\My Documents\\master\\Attosecond Pulses\\grating interferometry
     \\Simulations\\theoritical computations\\excitaYIONPROPABLITY_negative
     chearp_compressor_4000_points_interpolation.txt", "Table"];

ListPlot[DataTable, PlotRange → All, PlotJoined → True]

DataTable // MatrixForm

start = -50;
stop = 50;
amplitudestep = 0.0005;
phasestep = 0.0005;
fourierstep = 0.0005;

dim = Dimensions[DataTable];
FourierTransformFunction[v_] :=
    Position[DataTable,stop][[1,1]]
                ∑                  DataTable[[di, 2]] * Exp[i * 2 * π * v * DataTable[[di, 1]]];
  di=Position[DataTable,start][[1,1]]

FourierTranformTable = Table[FourierTransformFunction[v], {v, 0, 2, fourierstep}];

SpectralphaseTableWrapped = {};
Do[
  If[Re[FourierTranformTable[[di]]] < 0,
   SpectralphaseTableWrapped = Append[SpectralphaseTableWrapped,
     ArcTan[Im[FourierTranformTable[[di]]] / Re[FourierTranformTable[[di]]]] + π],
   SpectralphaseTableWrapped = Append[SpectralphaseTableWrapped,
     ArcTan[Im[FourierTranformTable[[di]]] / Re[FourierTranformTable[[di]]]]],
  {di, 1, Dimensions[FourierTranformTable][[1]]}];

SpectralAmplitudeTable = Abs[FourierTranformTable]^2;

dimnew1 = Dimensions[SpectralphaseTableWrapped];
SpectralphaseTableWrappedNew = {};
Do[
 SpectralphaseTableWrappedNew =
  Append[SpectralphaseTableWrappedNew, {di * phasestep - phasestep,
    SpectralphaseTableWrapped[[di]]}], {di, 1, dimnew1[[1]] - 1}]

ListPlot[SpectralphaseTableWrappedNew, PlotJoined → True]
ListPlot[SpectralAmplitudeTable, PlotJoined → True, PlotRange → All]

Export["D:\\My Documents\\master\\Attosecond Pulses\\grating interferometry\\
   Simulations\\theoritical computations\\excitaYIONPROPABLITY_spectralphasewrapped
   _negative chearp_new_code.txt", SpectralphaseTableWrappedNew, "TSV"]
```

APPENDICES

```
field = Table[{Re[
        Sum[DataTable[[di, 2]] * Exp[i * 2 * π * v * DataTable[[di, 1]]]],
          di=Position[DataTable,start][[1,1]]
          Position[DataTable,stop][[1,1]]
     Im[ Sum[DataTable[[di, 2]] *
          di=Position[DataTable,start][[1,1]]
        Exp[i * 2 * π * v * DataTable[[di, 1]]]]}, {v, 0, 4, amplitudestep}];
shift = 0;
n = 0;
xdim = Dimensions[field][[1]];
phase = Table[0, {xdim}];
Do[
  phase[[i]] = Im[Log[field[[i, 1]] + i * field[[i, 2]]]] + shift;
  If[phase[[i]] - phase[[i - 1]] ≤ -π / 2,
   n = n + 1, shift = n * π, phase[[i]] = phase[[i]] + π];
  If[phase[[i]] - phase[[i - 1]] ≥ π / 2, n = n - 1, shift = n * π, phase[[i]] = phase[[i]] - π];
  , {i, 2, Dimensions[field][[1]]}];

ListPlot[phase, PlotJoined → True]

dimnew1 = Dimensions[phase];
dimnew2 = Dimensions[SpectralAmplitudeTable];
SpectralphaseTableNew = {};
SpectralAmplitudeTableNew = {};
Do[
 SpectralphaseTableNew = Append[SpectralphaseTableNew,
   {di * phasestep - phasestep, phase[[di]]}], {di, 1, dimnew1[[1]] - 1}]
Do[
 SpectralAmplitudeTableNew =
  Append[SpectralAmplitudeTableNew, {di * amplitudestep - amplitudestep,
    SpectralAmplitudeTable[[di]]}], {di, 1, dimnew2[[1]] - 1}]
ListPlot[SpectralphaseTableNew, PlotJoined → True,
 AxesLabel → {"harmonic Frequency[fs^-1]", "spectral phase"}, PlotJoined → True,
 PlotRange → {All, All}, TextStyle → {FontFamily → "Times", FontSize → 20}]
ListPlot[SpectralAmplitudeTableNew, PlotJoined → True,
 AxesLabel → {"harmonic Frequency[fs^-1]", "spectral Amplitude"}, PlotRange → {All, All},
 PlotJoined → True, TextStyle → {FontFamily → "Times", FontSize → 20}]

- Graphics -

Export["D:\\My Documents\\master\\Attosecond Pulses\\grating interferometry\\
   Simulations\\theoritical computations\\excitaYIONPROPABLITY_spectralphaseunwrapped
   _compressor_negative_chearp_new_code.txt", SpectralphaseTableNew, "TSV"]
Export["D:\\My Documents\\master\\Attosecond Pulses\\grating interferometry\\
   Simulations\\theoritical computations\\excitaYIONPROPABLITY_spectralamplitude
   _compressor_negative_chearp_new_code.txt", SpectralAmplitudeTableNew, "TSV"]
```

Appendix D : Mathematica® code used to simulate the experiment

The following code is used for the calculations in Chapter 4.

Group velocity Dispersion-Grating

```
nm = 10^-9; (*m*)
d = 600; (*lines*)
Ng = d / 10^3; (*lines per m*)
l = 800. nm;(*fundamental wavelenght*)
thin = 0;  (*input angle*)
m = 1.; (*diffraction order*)
R = 31 ; (*grating distance from the second mirror*)
nm = 10^-9; (*m*)
A1 = 0.63472443;
A2 = 0.440647918;
A3 = 0.899007061;
B1 = 0.0665176613;
B2 = 0.115015076;
B3 = 9.90316809;
c = 300000000. * 10^6(*μm/s*);
d = 1. *10^3 (* geometrical path μm*);
k1[ω_] := ω / c;
k = 1;
fs = 10^-15;
w1 = 2 π 3 10^8 / (800 * 10^-9);
ni[λ_] := Sqrt[1 + A1 λ^2 / (-B1^2 + λ^2) + A2 λ^2 / (-B2^2 + λ^2) + A3 λ^2 / (-B3^2 + λ^2)]
n[ω_] := Sqrt[1 - 4 A1 c^2 π^2 / (-4 c^2 π^2 + B1^2 ω^2) - 4 A2 c^2 π^2 / (-4 c^2 π^2 + B2^2 ω^2) - 4 A3 c^2 π^2 / (-4 c^2 π^2 + B3^2 ω^2)];(*refractive index*)

D21[ω_] := 1 / 2
 (-2 1/c Sin[180/π (-ArcSin[1 m Ng / (1 + 2 k) - Sin[thin]])] * 360 c m Ng / ((1 + 2 k) ω^2 Sqrt[1 - (2 c m Ng π / ((1+2 k) ω) - Sin[thin])^2]) -
  k1[ω] Cos[180/π (-ArcSin[1 m Ng / (1 + 2 k) - Sin[thin]])] *
   (360 c m Ng / ((1 + 2 k) ω^2 Sqrt[1 - (2 c m Ng π / ((1+2 k) ω) - Sin[thin])^2]))^2 -
  k1[ω] * Sin[180/π (-ArcSin[1 m Ng / (1 + 2 k) - Sin[thin]])] * (720 c m Ng
     (2 c^2 m^2 Ng^2 π^2 - (ω + 2 k ω)^2 - 3 c (1 + 2 k) m Ng π ω Sin[thin] + (1 + 2 k)^2 ω^2 Sin[thin]^2)) /
   ((1 + 2 k)^2 ω^4 (ω + 2 k ω) (1 - (-2 c m Ng π / (ω + 2 k ω) + Sin[thin])^2)^(3/2)));
(*first pass from the grating*)
```

Appendices

```mathematica
D22[ω_] := 1/2 (-2 1/c Sin[0] *
      (360 c m Ng)/((1 + 2 k) ω^2 Sqrt[1 - ((2 c m Ng π)/((1+2 k) ω) - Sin[-ArcSin[(1 m Ng)/(1+2 k) - Sin[-ArcSin[(1 m Ng)/(1+2 k) - Sin[thin]]]]])^2]) -
    k1[ω] Cos[180/π 0] * ((360 c m Ng)/((1 + 2 k) ω^2 Sqrt[1 - ((2 c m Ng π)/((1+2 k) ω) - Sin[-ArcSin[(1 m Ng)/(1+2 k) - Sin[thin]]])^2]))^2 -
    k1[ω] * Sin[180/π (0)] * (720 c m Ng
        (2 c^2 m^2 Ng^2 π^2 - (ω + 2 k ω)^2 - 3 c (1 + 2 k) m Ng π ω Sin[-ArcSin[(1 m Ng)/(1 + 2 k) - Sin[thin]]] +
          (1 + 2 k)^2 ω^2 Sin[-ArcSin[(1 m Ng)/(1 + 2 k) - Sin[-ArcSin[(1 m Ng)/(1 + 2 k) - Sin[thin]]]]]^2)) /
      ((1 + 2 k)^2 ω^4 (ω + 2 k ω) (1 - (-(2 c m Ng π)/(ω + 2 k ω) + Sin[thin])^2)^(3/2)));

Pulseduration[ω_] := Abs[25 Sqrt[1 + (4 Log[2] ((D21[ω] + D22[ω]) * 10^30)/25^2)^2]];

(*second pass from the grating*)

Plot[Pulseduration[ω], {ω, (2 π c)/1.5, (2 π c)/.1}, PlotRange → All,
  AxesLabel → {"Frequency [fs^-1]", "Pulse Duration [fs]"},
  TextStyle → {FontFamily → "Times", FontSize → 20}];

GroupVelocityDispersions = {};
Do[
 GroupVelocityDispersions = Append[GroupVelocityDispersions,
   {(1/(1 + 2 k))^-1, (1/2 (-2 1/c Sin[180/π (-ArcSin[(1 m Ng)/(1 + 2 k) - Sin[thin]])] *
        (360 c m Ng)/((1 + 2 k) ((2 π c)/(.8/(2 k+1)))^2 Sqrt[1 - ((2 c m Ng π)/((1+2 k) (2 π c)/(.8/(2 k+1))) - Sin[thin])^2]) -
```

$$k1\left[\frac{2\pi c}{(.8/(2k+1))}\right]\cos\left[\frac{180}{\pi}\left(-\arcsin\left[\frac{1\,m\,Ng}{1+2k}-\sin[thin]\right]\right)\right]*\left(\frac{360\,c\,m\,Ng}{(1+2k)\left(\frac{2\pi c}{(.8/(2k+1))}\right)^2\sqrt{1-\left(\frac{2\,c\,m\,Ng\,\pi}{(1+2k)\,\frac{2\pi c}{(.8/(2k+1))}}-\sin[thin]\right)^2}}\right)^2-$$

$$k1\left[\frac{2\pi c}{(.8/(2k+1))}\right]*\sin\left[\frac{180}{\pi}\left(-\arcsin\left[\frac{1\,m\,Ng}{1+2k}-\sin[thin]\right]\right)\right]*\left(720\,c\,m\,Ng\left(2\,c^2\,m^2\,Ng^2\,\pi^2-\left(\frac{2\pi c}{(.8/(2k+1))}+2k\,\frac{2\pi c}{(.8/(2k+1))}\right)^2-3\,c\,(1+2k)\,m\,Ng\,\pi\,\frac{2\pi c}{(.8/(2k+1))}\sin[thin]+(1+2k)^2\left(\frac{2\pi c}{(.8/(2k+1))}\right)^2\sin[thin]^2\right)\right)\Big/\left((1+2k)^2\left(\frac{2\pi c}{(.8/(2k+1))}\right)^4\left(\frac{2\pi c}{(.8/(2k+1))}+2k\,\frac{2\pi c}{(.8/(2k+1))}\right)\left(1-\left(-\frac{2\,c\,m\,Ng\,\pi}{\frac{2\pi c}{(.8/(2k+1))}+2k\,\frac{2\pi c}{(.8/(2k+1))}}+\sin[thin]\right)^2\right)^{3/2}\right)+$$

$$\left(1/2\left(-2\,\frac{1}{c}\sin[0]*(360\,c\,m\,Ng)\Big/\left((1+2k)\left(\frac{2\pi c}{(.8/(2k+1))}\right)^2\sqrt{1-\left(\frac{2\,c\,m\,Ng\,\pi}{(1+2k)\,\frac{2\pi c}{(.8/(2k+1))}}-\sin\left[-\arcsin\left[\frac{1\,m\,Ng}{1+2k}-\sin[thin]\right]\right]\right)^2}\right)-k1\left[\frac{2\pi c}{(.8/(2k+1))}\right]\cos\left[\frac{180}{\pi}\,0\right]*\left(360\,c\,m\,Ng\right)\Big/\left((1+2k)\left(\frac{2\pi c}{(.8/(2k+1))}\right)^2\sqrt{\left(1-\left(\frac{2\,c\,m\,Ng\,\pi}{(1+2k)\,\frac{2\pi c}{(.8/(2k+1))}}-\sin\left[-\arcsin\left[\frac{1\,m\,Ng}{1+2k}-\sin\left[-\arcsin\left[\frac{1\,m\,Ng}{1+2k}-\sin[thin]\right]\right]\right]\right]\right)^2\right)\right)^2-k1\left[\frac{2\pi c}{(.8/(2k+1))}\right]*\sin\left[\frac{180}{\pi}\,(0)\right]*\left(720\,c\,m\,Ng\left(2\,c^2\,m^2\,Ng^2\,\pi^2-\left(\frac{2\pi c}{(.8/(2k+1))}+2k\,\frac{2\pi c}{(.8/(2k+1))}\right)^2-3\,c\,(1+2k)\,m\,Ng\,\pi\,\frac{2\pi c}{(.8/(2k+1))}\sin\left[-\arcsin\left[\frac{1\,m\,Ng}{1+2k}-\sin[thin]\right]\right]+(1+2k)^2\left(\frac{2\pi c}{(.8/(2k+1))}\right)^2\sin\left[-\arcsin\left[\frac{1\,m\,Ng}{1+2k}-\sin\left[-\arcsin\left[\frac{1\,m\,Ng}{1+2k}-\sin[thin]\right]\right]\right]\right]^2\right)\Big/$$

$$\left((1+2k)^2\left(\frac{2\pi c}{(.8/(2k+1))}\right)^4\left(\frac{2\pi c}{(.8/(2k+1))}+2k\,\frac{2\pi c}{(.8/(2k+1))}\right)\left(1-\left(-\frac{2\,c\,m\,Ng\,\pi}{\frac{2\pi c}{(.8/(2k+1))}+2k\,\frac{2\pi c}{(.8/(2k+1))}}+\text{Sin}[\text{thin}]\right)^2\right)^{3/2}\right)\Bigg)\Bigg)\Bigg)*10^{30}\Big\},\ \{k,\ 0,\ 15$$

```
GroupVelocityDispersions // MatrixForm(*the results is harmonics vs fs^2*)

GVD = ListPlot[GroupVelocityDispersions, PlotJoined → False,
  PlotRange → {{2, 11}, {-5, 0}}, AxesLabel → {"Number of Harmonics", "D2 [fs^2]"},
  PlotLabel -> "GVD", TextStyle → {FontFamily → "Times", FontSize → 20}]
```

- Graphics -

```
Export["E:\\My Documents\\master\\Attosecond Pulses\\Charambidis\\project\\group
   meeting presentation\\gratingGVD.tif", GVD, "TIFF", ImageSize → {1000, 1000}]

pulseduration = {};
Do[
  pulseduration = Append[pulseduration, {(1/(1+2 di))^-1,
    Abs[25 Sqrt[1 + (4 Log[2] GroupVelocityDispersions[[di + 1, 2]]/25^2)^2]]}], {di, 1, 15}];
pulseduration // MatrixForm(*the results is harmonics vs fs^2*)

pulseDUR = ListPlot[pulseduration,
  PlotJoined → False, AxesLabel → {"Number of Harmonic", "Δt [fs]"},
  PlotLabel -> "Pulsedurations", PlotRange → {{3, 12}, All},
  TextStyle → {FontFamily → "Times", FontSize → 20}, AxesOrigin → {3, 25}]
```

- Graphics -

```
(*Export["E:\\My Documents\\master\\Attosecond Pulses\\Charambidis
    \\project\\group meeting presentation\\pulsedurationGratingGVD.tif",
  pulseDUR,"TIFF",ImageSize→{1000,1000}]*)
```

Group velocity Dispersion-Fused Silica(SiO2)

Fitting refractive-index data with the Sellmeier dispersion formula

```
nm = 10^-9; (*m*)
A1 = 0.63472443;
A2 = 0.440647918;
A3 = 0.899007061;
B1 = 6.65176613*10^-2;
B2 = 1.15015076*10^-1;
B3 = 9.90316809;
c = 3*10^14 / 10^15 (*μm/fs*);
d = 1*10^3 (* geometrical path μm*);
```

$$ni[\lambda\_] := \sqrt{1+\frac{A1\,\lambda^2}{-B1^2+\lambda^2}+\frac{A2\,\lambda^2}{-B2^2+\lambda^2}+\frac{A3\,\lambda^2}{-B3^2+\lambda^2}}$$

$$n[\omega\_] := \sqrt{1-\frac{4\,A1\,c^2\,\pi^2}{-4\,c^2\,\pi^2+B1^2\,\omega^2}-\frac{4\,A2\,c^2\,\pi^2}{-4\,c^2\,\pi^2+B2^2\,\omega^2}-\frac{4\,A3\,c^2\,\pi^2}{-4\,c^2\,\pi^2+B3^2\,\omega^2}}\ ;(*\text{refractive index}*)$$

$$l[\omega\_] := 2*d*\sqrt{1-\frac{4\,A1\,c^2\,\pi^2}{-4\,c^2\,\pi^2+B1^2\,\omega^2}-\frac{4\,A2\,c^2\,\pi^2}{-4\,c^2\,\pi^2+B2^2\,\omega^2}-\frac{4\,A3\,c^2\,\pi^2}{-4\,c^2\,\pi^2+B3^2\,\omega^2}}\ ;(*\text{optical path}*)$$

```
D2[ω_] := 2 d/c ( -(ω (8 A1 B1^2 c^2 π^2 ω/(-4 c^2 π^2+B1^2 ω^2)^2 + 8 A2 B2^2 c^2 π^2 ω/(-4 c^2 π^2+B2^2 ω^2)^2 + 8 A3 B3^2 c^2 π^2 ω/(-4 c^2 π^2+B3^2 ω^2)^2)^2)/(4 (1 - 4 A1 c^2 π^2/(-4 c^2 π^2+B1^2 ω^2) - 4 A2 c^2 π^2/(-4 c^2 π^2+B2^2 ω^2) - 4 A3 c^2 π^2/(-4 c^2 π^2+B3^2 ω^2))^(3/2)) +
  (ω (-(32 A1 B1^4 c^2 π^2 ω^2/(-4 c^2 π^2 + B1^2 ω^2)^3) + 8 A1 B1^2 c^2 π^2/(-4 c^2 π^2 + B1^2 ω^2)^2 - 32 A2 B2^4 c^2 π^2 ω^2/(-4 c^2 π^2 + B2^2 ω^2)^3 +
  8 A2 B2^2 c^2 π^2/(-4 c^2 π^2 + B2^2 ω^2)^2 - 32 A3 B3^4 c^2 π^2 ω^2/(-4 c^2 π^2 + B3^2 ω^2)^3 + 8 A3 B3^2 c^2 π^2/(-4 c^2 π^2 + B3^2 ω^2)^2)) /
  (2 Sqrt[1 - 4 A1 c^2 π^2/(-4 c^2 π^2 + B1^2 ω^2) - 4 A2 c^2 π^2/(-4 c^2 π^2 + B2^2 ω^2) - 4 A3 c^2 π^2/(-4 c^2 π^2 + B3^2 ω^2)]) +
  (8 A1 B1^2 c^2 π^2 ω/(-4 c^2 π^2+B1^2 ω^2)^2 + 8 A2 B2^2 c^2 π^2 ω/(-4 c^2 π^2+B2^2 ω^2)^2 + 8 A3 B3^2 c^2 π^2 ω/(-4 c^2 π^2+B3^2 ω^2)^2)/
  Sqrt[1 - 4 A1 c^2 π^2/(-4 c^2 π^2+B1^2 ω^2) - 4 A2 c^2 π^2/(-4 c^2 π^2+B2^2 ω^2) - 4 A3 c^2 π^2/(-4 c^2 π^2+B3^2 ω^2)] ); (*D2[ω] = 2 d/c ∂^2 (ω n[ω_])/∂ ω^2 *)

Plot[Abs[D2[ω]], {ω, 2 π c/(0.8), 2 π c/(0.8/5)}, PlotRange → All,
 AxesLabel → {"angular frenquency [fsec^-1]", "D2 [fs^2]"}]

GroupVelocityDispersionsFS = {};
Do[
 GroupVelocityDispersionsFS = Append[GroupVelocityDispersionsFS, {(1/(1 + 2 k))^-1,
  2 d/c ( -((2 π c/(.8/(2 k + 1))) (8 A1 B1^2 c^2 π^2 (2 π c/(.8/(2 k+1)))/(-4 c^2 π^2 + B1^2 (2 π c/(.8/(2 k+1)))^2)^2 + 8 A2 B2^2 c^2 π^2 (2 π c/(.8/(2 k+1)))/(-4 c^2 π^2 + B2^2 (2 π c/(.8/(2 k+1)))^2)^2 +
  8 A3 B3^2 c^2 π^2 (2 π c/(.8/(2 k+1)))/(-4 c^2 π^2 + B3^2 (2 π c/(.8/(2 k+1)))^2)^2)^2) / (4 (1 - 4 A1 c^2 π^2/(-4 c^2 π^2 + B1^2 (2 π c/(.8/(2 k+1)))^2) -
  4 A2 c^2 π^2/(-4 c^2 π^2 + B2^2 (2 π c/(.8/(2 k+1)))^2) - 4 A3 c^2 π^2/(-4 c^2 π^2 + B3^2 (2 π c/(.8/(2 k+1)))^2))^(3/2)) +
  (2 π c/(.8/(2 k + 1))) (-(32 A1 B1^4 c^2 π^2 (2 π c/(.8/(2 k+1)))^2/(-4 c^2 π^2 + B1^2 (2 π c/(.8/(2 k+1)))^2)^3) + 8 A1 B1^2 c^2 π^2/(-4 c^2 π^2 + B1^2 (2 π c/(.8/(2 k+1)))^2)^2 -
  32 A2 B2^4 c^2 π^2 (2 π c/(.8/(2 k+1)))^2/(-4 c^2 π^2 + B2^2 (2 π c/(.8/(2 k+1)))^2)^3 + 8 A2 B2^2 c^2 π^2/(-4 c^2 π^2 + B2^2 (2 π c/(.8/(2 k+1)))^2)^2 -
  32 A3 B3^4 c^2 π^2 (2 π c/(.8/(2 k+1)))^2/(-4 c^2 π^2 + B3^2 (2 π c/(.8/(2 k+1)))^2)^3 + 8 A3 B3^2 c^2 π^2/(-4 c^2 π^2 + B3^2 (2 π c/(.8/(2 k+1)))^2)^2) /
  (2 Sqrt[1 - 4 A1 c^2 π^2/(-4 c^2 π^2 + B1^2 (2 π c/(.8/(2 k+1)))^2) - 4 A2 c^2 π^2/(-4 c^2 π^2 + B2^2 (2 π c/(.8/(2 k+1)))^2) -
  4 A3 c^2 π^2/(-4 c^2 π^2 + B3^2 (2 π c/(.8/(2 k+1)))^2)]) +
  (8 A1 B1^2 c^2 π^2 (2 π c/(.8/(2 k+1)))/(-4 c^2 π^2+B1^2 (2 π c/(.8/(2 k+1)))^2)^2 + 8 A2 B2^2 c^2 π^2 (2 π c/(.8/(2 k+1)))/(-4 c^2 π^2+B2^2 (2 π c/(.8/(2 k+1)))^2)^2 +
  8 A3 B3^2 c^2 π^2 (2 π c/(.8/(2 k+1)))/(-4 c^2 π^2+B3^2 (2 π c/(.8/(2 k+1)))^2)^2)/
  Sqrt[1 - 4 A1 c^2 π^2/(-4 c^2 π^2+B1^2 (2 π c/(.8/(2 k+1)))^2) - 4 A2 c^2 π^2/(-4 c^2 π^2+B2^2 (2 π c/(.8/(2 k+1)))^2) - 4 A3 c^2 π^2/(-4 c^2 π^2+B3^2 (2 π c/(.8/(2 k+1)))^2)] )}],
 {k, 0, 15}]
GroupVelocityDispersionsFS // MatrixForm(*the results is harmonics vs fs^2*)

FSGVD = ListPlot[GroupVelocityDispersionsFS,
  PlotJoined → False, AxesLabel → {"Number of Harmonics", "D2 [fs^2]"},
  PlotLabel -> "GVD", TextStyle → {FontFamily → "Times", FontSize → 20}]
```

APPENDICES

```
pulsedurationFS = {};
Do[
  pulsedurationFS = Append[pulsedurationFS, {(1/(1 + 2 di))^-1, 56 / Sqrt[1 + 2 di]
      Sqrt[1 + (4 Log[2] GroupVelocityDispersionsFS[[di + 1, 2]] / (56 / Sqrt[1 + 2 di])^2)^2]}], {di, 0, 15}];
pulsedurationFS // MatrixForm(*the results is harmonics vs fs*)

FSPulseDuration = ListPlot[pulsedurationFS,
  PlotJoined → False, AxesLabel → {"Number of Harmonic", "Δt [fs]"},
  PlotLabel -> "Pulsedurations", TextStyle → {FontFamily → "Times", FontSize → 20}]
```

Group velocity Dispersion-LiF

Fitting refractive-index data with the Sellmeier dispersion formula

```
nm = 10^-9; (*m*)
c = 3 * 10^17 / 10^15 (*nm/fs*);
dLiF = 2 * 10^6 (* geometrical path nm*);
A = 1.38762;
B = 10.3488;
M = -32039.6292;
G = 650341747.8;

ni[λ_] := A + B / λ^2 + M / λ^4 + G / λ^6;
n[ω_] := A + B / (2 π c / ω)^2 + M / (2 π c / ω)^4 + G / (2 π c / ω)^6 ;(*refractive index*)


l[ω_] := dLiF * n[ω] ; (*optical path*)
```

$$D2[\omega\_] := \frac{dLiF}{c}\left(\frac{B\,\omega}{c^2\,\pi^2} + \frac{M\,\omega^3}{2\,c^4\,\pi^4} + \frac{3\,G\,\omega^5}{16\,c^6\,\pi^6} + \omega\left(\frac{B}{2\,c^2\,\pi^2} + \frac{3\,M\,\omega^2}{4\,c^4\,\pi^4} + \frac{15\,G\,\omega^4}{32\,c^6\,\pi^6}\right)\right);$$

$$(*D2[\omega] = \frac{2\,d}{c}\,\frac{\partial^2\,(\omega\ n[\omega\_])}{\partial\,\omega^2}\,*)$$

```
Plot[Abs[D2[ω]], {ω, 2 π c / (800), 2 π c / (800 / 30)}, PlotRange → All,
 AxesLabel → {"angular frenquency [fsec^-1]", "D2 [fs^2]"}]
```

```
- Graphics -
```

```
GroupVelocityDispersionsLiF = {};
Do[
 GroupVelocityDispersionsLiF = Append[GroupVelocityDispersionsLiF,
   {(1 / (1 + 2 k))^-1, dLiF / c (B 2 π c / (800 / (2 k + 1)) / (2 c^2 π^2) +
       M (2 π c / (800 / (2 k + 1)))^3 / (2 c^4 π^4) +
       3 G (2 π c / (800 / (2 k + 1)))^5 / (16 c^6 π^6) +
       2 π c / (800 / (2 k + 1)) (B / (2 c^2 π^2) +
         3 M (2 π c / (800 / (2 k + 1)))^2 / (4 c^4 π^4) +
         15 G (2 π c / (800 / (2 k + 1)))^4 / (32 c^6 π^6)))}], {k, 0, 15}]
GroupVelocityDispersionsLiF // MatrixForm(*the results is harmonics vs fs^2*)

LiFGVD = ListPlot[GroupVelocityDispersionsLiF,
  PlotJoined → False, AxesLabel → {"Number of Harmonics", "D2 [fs^2]"},
  PlotLabel -> "GVD", TextStyle → {FontFamily → "Times", FontSize → 20}]
```

```
- Graphics -
```

```
Export["E:\\My Documents\\master\\Attosecond Pulses\\Charambidis\\project\\group
   meeting presentation\\FusedSilicaGVD.tif", FSGVD, "TIFF", ImageSize → {1000, 1000}]

pulsedurationFS = {};
Do[
  pulsedurationFS = Append[pulsedurationFS, {(1 / (1 + 2 di))^-1, 56 / Sqrt[1 + 2 di]
      Sqrt[1 + (4 Log[2] GroupVelocityDispersionsFS[[di + 1, 2]] / (56 / Sqrt[1 + 2 di])^2)^2]}], {di, 0, 15}];
pulsedurationFS // MatrixForm(*the results is harmonics vs fs*)

FSPulseDuration = ListPlot[pulsedurationFS,
  PlotJoined → False, AxesLabel → {"Number of Harmonic", "Δt [fs]"},
  PlotLabel -> "Pulsedurations", TextStyle → {FontFamily → "Times", FontSize → 20}]
```

Group velocity Dispersion-Adding negative chearp in the compressor

```
pulsedurationFSnegativechearp = {};
Do[
  pulsedurationFSnegativechearp =
    Append[pulsedurationFSnegativechearp, {(1/(1 + 2 di))^-1, 56 / Sqrt[1 + 2 di] * √(1 + (4 Log[2
          (GroupVelocityDispersionsFS[[di + 1, 2]] - GroupVelocityDispersionsFS[[2,
              2]]) / (56 / Sqrt[1 + 2 di])^2)^2)}], {di, 1, 15)];
pulsedurationFSnegativechearp // MatrixForm(*the results is harmonics vs fs*)
```

3	32.3316
5	420.851
7	$92.188 - 1.04503 \times 10^7 i$
9	299.025
11	13164.4
13	$125.631 - 16770. i$
15	$134.953 + 2048.25 i$
17	1714.92
19	472.755
21	289.702
23	235.155
25	215.253
27	208.164
29	206.737
31	208.108

```
FSPulseDuration = ListPlot[pulsedurationFS,
  PlotJoined → False, AxesLabel → {"Number of Harmonic", "Δt [fs]"},
  PlotLabel -> "Pulsedurations", TextStyle → {FontFamily → "Times", FontSize → 20}]
```

Fourier Tranform with chearp and time delay

```
fs = 10^-15;
wl = 2. π 3. 10^8 / (800. * 10^-9);
ph1 = ph3 = ph7 = ph5 = 0;
step = 0.025 fs;
start = -25 fs;
stop = 25 fs;

DataTable = Table[NIntegrate[
    (Exp[-((t - τ) / (56 fs / (2 Sqrt[Log[2]])))^2]^3 * pulsedurationFSnegativechearp[[1, 2]] fs / (2 Sqrt[Log[2]]) /
      ((((pulsedurationFSnegativechearp[[1, 2]] fs / (2 Sqrt[Log[2]]))^4 + ((GroupVelocityDispersionsFS[[2,
            2]] - GroupVelocityDispersionsFS[[2, 2]]) * fs^2)^2)^(1 / 4)) *
     Exp[-(t / (pulsedurationFSnegativechearp[[1, 2]] fs / (2 Sqrt[Log[2]])))^2] Cos[3 ph1 - ph3 - 3 wl τ +
      (-((GroupVelocityDispersionsFS[[2, 2]] - GroupVelocityDispersionsFS[[2, 2]]) fs^2) /
         (2 ((56 / Sqrt[3] fs / (2 Sqrt[Log[2]]))^4 + (GroupVelocityDispersionsFS[[2, 2]] fs^2)^2)))
       t^2 + 1/2 ArcTan[1 / (56/Sqrt[3] fs / (2 Sqrt[Log[2]]))^2 ((GroupVelocityDispersionsFS[[2, 2]] -
           GroupVelocityDispersionsFS[[2, 2]]) fs^2)]] + Exp[-((t - τ) / (56 fs / (2 Sqrt[Log[2]])))^2]^5 *
    .25 pulsedurationFS[[3,2]] fs / (2 Sqrt[Log[2]]) /
     Sqrt[(pulsedurationFS[[3,2]] fs / (2 Sqrt[Log[2]]))^4 + (GroupVelocityDispersionsFS[[3, 2]] * fs^2)^2]
```

APPENDICES

$$\text{Exp}\left[-\left(t \Big/ \left(\frac{\text{pulsedurationFS}[[3,\,2]]\ \text{fs}}{2\sqrt{\text{Log}[2]}}\right)\right)^2\right]$$
$$\text{Cos}\Big[5\,\text{ph1} - \text{ph5} - 5\,\text{w1}\,(\tau - 70\,\text{fs}) +$$
$$\left(-\frac{(\text{GroupVelocityDispersionsFS}[[3,\,2]])\ \text{fs}^2}{2\left(\left(\frac{56/\text{Sqrt}[5]\ \text{fs}}{2\sqrt{\text{Log}[2]}}\right)^4 + (\text{GroupVelocityDispersionsFS}[[3,\,2]]\ \text{fs}^2)^2\right)}\,(t - 70\,\text{fs})^2 +\right.$$
$$\left.\frac{1}{2}\,\text{ArcTan}\Big[\frac{\text{GroupVelocityDispersionsFS}[[3,\,2]]}{\left(\frac{56/\text{Sqrt}[5]\ \text{fs}}{2\sqrt{\text{Log}[2]}}\right)^2}\Big]\right]\Big] +$$
$$\text{Exp}\left[-\left((t - \tau) \Big/ \left(\frac{56\,\text{fs}}{2\sqrt{\text{Log}[2]}}\right)\right)^{2\ 7}\right] * 0. * \text{Exp}\Big[$$
$$-\left(t \Big/ \left(\frac{\text{pulsedurationFSnegativechearp}[[1,\,2]]\ \text{fs}}{2\sqrt{\text{Log}[2]}}\right)\right)^2\Big]\ \text{Cos}\Big[7\,\text{ph1} - \text{ph7} - 7\,\text{w1}\,\tau +$$
$$\left(-((\text{GroupVelocityDispersionsFS}[[4,\,2]] - \text{GroupVelocityDispersionsFS}[[2,\,2]])\right.$$
$$\text{fs}^2) \Big/ \left(2\left(\left(\frac{56\,/\,\text{Sqrt}[7]\ \text{fs}}{2\sqrt{\text{Log}[2]}}\right)^4 + (\text{GroupVelocityDispersionsFS}[[1,\,2]]\ \text{fs}^2)^2\right)\right)$$
$$t^2 + \frac{1}{2}\,\text{ArcTan}\Big[\frac{1}{\left(\frac{56/\text{Sqrt}[7]\ \text{fs}}{2\sqrt{\text{Log}[2]}}\right)^2}((\text{GroupVelocityDispersionsFS}[[4,\,2]] -$$
$$\left.\left.\text{GroupVelocityDispersionsFS}[[2,\,2]])\ \text{fs}^2)\Big]\right]\Big],$$
$$\{t,\,-250\,\text{fs},\,250\,\text{fs}\}\Big],\ \{\tau,\,\text{start},\,\text{stop},\,\text{step}\}\Big];$$

```
ListPlot[DataTable, PlotRange → All, PlotJoined → True]
```

```
dim = Dimensions[DataTable];
DataTablenew = {};
Do[DataTablenew = Append[DataTablenew, {start + di step, DataTable[[di + 1]]}],
  {di, 0, dim[[1]] - 1}];

ListPlot[DataTablenew, PlotRange → All, PlotJoined → True]
```

```
start = -2.4975000000000002`*^-14;
stop = 2.5000000000000007`*^-14;
amplitudestep = 0.001 * 10^15;
phasestep = 0.001 * 10^15;

dim = Dimensions[DataTablenew];
FourierTransformFunction[v_] := Sum[DataTablenew[[di, 2]] *
    Exp[i * 2 * π * v * DataTablenew[[di, 1]]], {di, Position[DataTablenew, start][[1,1]], Position[DataTablenew, stop][[1,1]]}];


SpectralphaseTable =
  Table[ArcTan[Im[FourierTransformFunction[v]] / Re[FourierTransformFunction[v]]],
   {v, 0, 2 * 1 / fs, phasestep}];
SpectralAmplitudeTable = Table[Abs[FourierTransformFunction[v]]^2,
   {v, 0, 2 * 1 / fs, amplitudestep}];



dimnew1 = Dimensions[SpectralphaseTable];
SpectralphaseTableWrapped = {};
Do[
 SpectralphaseTableWrapped = Append[SpectralphaseTableWrapped,
   {di * phasestep - phasestep, SpectralphaseTable[[di]]}], {di, 1, dimnew1[[1]] - 1}]

ListPlot[SpectralphaseTableWrapped, PlotJoined → True, PlotRange → {All, All}]
ListPlot[SpectralAmplitudeTable, PlotJoined → True, PlotRange → All]

field = Table[{Re[Sum[DataTablenew[[di, 2]] *
        Exp[i * 2 * π * v * DataTablenew[[di, 1]]], {di, Position[DataTable, start][[1,1]], Position[DataTable, stop][[1,1]]}],
     Im[Sum[DataTablenew[[di, 2]] *
        Exp[i * 2 * π * v * DataTablenew[[di, 1]]], {di, Position[DataTable, start][[1,1]], Position[DataTable, stop][[1,1]]}]]}, {v, 0, 4, amplitudestep}];
shift = 0;
n = 0;
xdim = Dimensions[field][[1]];
phase = Table[0, {xdim}];
Do[
  phase[[i]] = Im[Log[field[[i, 1]] + i * field[[i, 2]]]] + shift;
  If[phase[[i]] - phase[[i - 1]] ≤ -π / 2,
   n = n + 1, shift = n * π, phase[[i]] = phase[[i]] + π];
  If[phase[[i]] - phase[[i - 1]] ≥ π / 2, n = n - 1, shift = n * π, phase[[i]] = phase[[i]] - π];
  , {i, 2, Dimensions[field][[1]]}];

ListPlot[phase, PlotJoined → True]

dimnew1 = Dimensions[phase];
dimnew2 = Dimensions[SpectralAmplitudeTable];
SpectralphaseTableNew = {};
SpectralAmplitudeTableNew = {};
Do[
 SpectralphaseTableNew = Append[SpectralphaseTableNew,
   {di * phasestep - phasestep, phase[[di]]}], {di, 1, dimnew1[[1]] - 1}]
Do[
 SpectralAmplitudeTableNew =
  Append[SpectralAmplitudeTableNew, {di * amplitudestep - amplitudestep,
    SpectralAmplitudeTable[[di]]}], {di, 1, dimnew2[[1]] - 1}]
ListPlot[SpectralphaseTableNew, PlotJoined → True,
 AxesLabel → {"harmonic Frequency[fs^-1]", "spectral phase"}, PlotJoined → True,
 PlotRange → {All, All}, TextStyle → {FontFamily → "Times", FontSize → 20}]
ListPlot[SpectralAmplitudeTableNew, PlotJoined → True,
 AxesLabel → {"harmonic Frequency[fs^-1]", "spectral Amplitude"}, PlotRange → {All, All},
 PlotJoined → True, TextStyle → {FontFamily → "Times", FontSize → 20}]
```

Appendix E: Mathematica® code used for the pulse reconstruction

Pulse Reconstruction

```
SpectralAmplitude = Import["D:\\My Documents\\master\\
     Attosecond Pulses\\fifth harmonic spectral amplitude.txt", "Table"];
SpectralPhase = Import["D:\\My Documents\\master\\Attosecond
     Pulses\\fifth harmonic spectral phases.txt", "Table"];
ListPlot[SpectralAmplitude, PlotRange → All, PlotJoined → True]
ListPlot[SpectralPhase, PlotRange → All, PlotJoined → True]

                    Dimensions[SpectralAmplitude][[1]]
Pulse[t_] :=              ∑                √SpectralAmplitude[[i, 2]] *
                          i=1

    Exp[i (SpectralAmplitude[[i, 1]] t - 2 * π * SpectralPhase[[i, 2]])];

dimnew1 = Dimensions[PulseTable];
PulseTableNew = {};
Do[
 PulseTableNew = Append[PulseTableNew, {-200 + (di * .1) - .1, PulseTable[[di]]}],
 {di, 1, dimnew1[[1]] - 1}]
ListPlot[PulseTableNew, PlotRange → All, PlotJoined → True]
ListPlot[PulseTable, PlotJoined → True,
 AxesLabel → {"harmonic Frequency[fs^-1]", "spectral phase"}, PlotJoined → True,
 PlotRange → {All, All}, TextStyle → {FontFamily → "Times", FontSize → 20}]
```

Appendix F: Micro-channel Plate Detector

Micro-channel plate (MCP) assemblies are widely used to detect electrons, ions and photons and to do spectroscopy of their impact position ("imaging") and/or time-of-flight ("timing") with respect to an 5 external trigger. There are different approaches to retrieve the two-dimensional (2d) position and time information from the MCP for single particle counting. Often both, time and position decoding, of a detected particle or even a particle shower (e.g. for imaging fragment patterns of a particle break-up) is important. Such tasks are found in atomic and molecular science as well as in surface and material science applications.

An MCP can be used for photon and particle imaging. Furthermore, due to the small size of each individual electron multiplier (each tube) the timing of the photon/particle impact can be determined very accurately (precision of better than 100 psec).The main purpose of MCP is low-level light amplification. A photo-cathode converts visible photons to electrons, which are projected on the MCP. Behind the MCP a phosphor screen converts the

"amplified" charge cloud to photons again, with a high effective light gain. A single MCP stage shows saturation effects in the pore so that for ultra-low light-level two or more MCP are stacked in series. Thus, individual photons can be made visible, with gains of 10 to100 million.

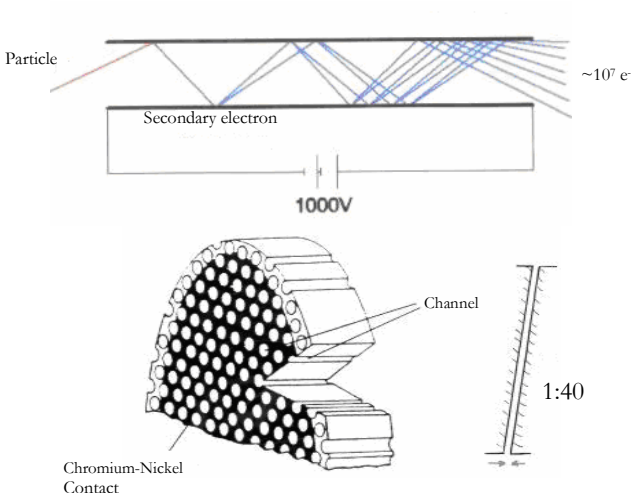

Figure 0-1: ***top:*** one MCP channel and **Bottom:** top view of a MCP

Appendix G: Data acquisition Software

The data acquisition software synchronizes the piezoelectric crystal with the oscilloscope. In this section we will give a brief but exact description how this program works.

The **Figure 0-1** shows the interface of the software where all the basic parameters are introduced. The option "Interval number" denotes the number of steps that the motor has to move. The option "unitinterval" denotes the step of the motor in microns. The option "Average Value" is the number of pulses that the oscilloscope averaging and gives a single value back to the program for recording. The value "timeout" is the time that the motor has to move to the next step. After all this values are filled then press "START" button.

The second screen (**Figure 0-1**(b)) is the communication page with the oscilloscope. There is an option which gives the possibility to choose which channel of the oscilloscope is needed for monitoring. Then the screen of the oscilloscope is presented on the screen.

Using the vertical cursors is defined the area that should be recorded. Then press the "Finish" button and the program starts the recording of the data.

(a)

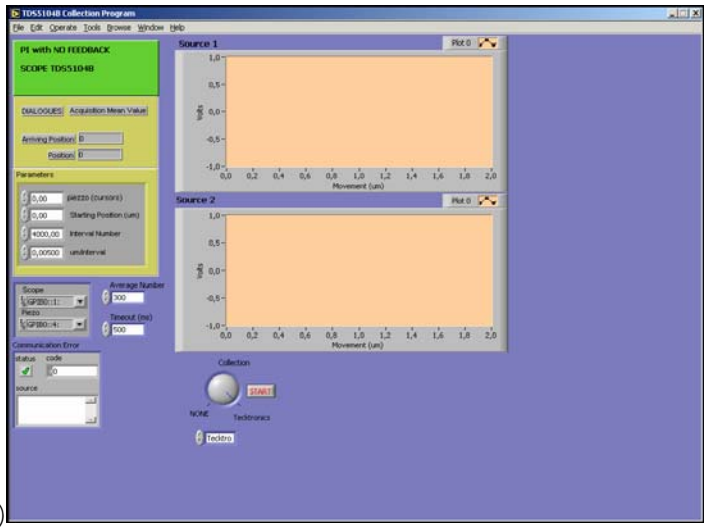

(b)

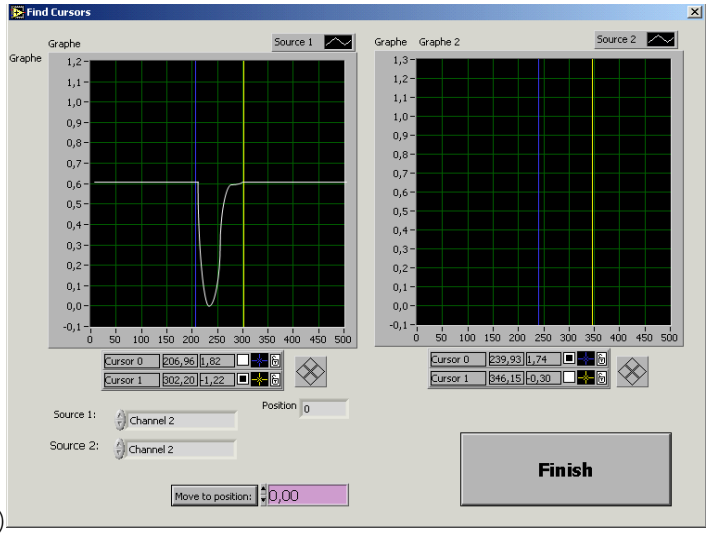

Figure 0-1: (a) First screen of the software that all the basic parameter are inserted,(b) second screen where the selection of the recorded area takes place .

References

1 DeMaria A J *et al , Appl. Phys. Lett.,* **12 ,**483 (1974)

2 Shank C V and Ippen E P ,*Appl. Phys. Lett,.* **24 ,**273, (1974)

3 Fork R L *et al* , *Opt. Lett.* **12,** 483,(1987)

4 Steinmeyer G *et al*, *Science* **286,** 1507, (1999)

5 Hansch T W , *Opt. Commun.* **80,** 70,(1990)

6 Farkas G and Toth C , *Phys. Lett.* A ,**168 ,**447,(1992)

7 Harris S E *et al, Opt. Commun.,* **100,** 487,(1993)

8 Kaplan A E,*Phys. Rev. Lett.,***73,**1243(1994)

9 Harris S E and Sokolov A V, *Phys. Rev.* A, **55,**R4019,(1997)

10 Harris S E and Sokolov A V,*Phys. Rev. Lett.,* **81,** 2894,(1998)

11 Sansone G. *et al, Science,* **314,**443,(2006)

12 Ivanov M *et al , Phys. Rev. Lett.,* **74 ,**2933,(1995)

13 Platonenko V T and Strelkov V V , *J. Opt. Soc. Am.* B **16,** 435,(1999)

14 N. A Papadogiannis *et al.*, *Phys. Rev. Let.*, **83**, 4289, (1999).

15 P. B. Corkum, *Nature*, **403**, 845, (2000).

16 N. A. Papadogiannis, and D. Charalambidis, *Phys. Rev. Lett.*, **87**, 109402, (2001).

17 G. Tempea *et al.*, *Phys. Rev. Lett.*, **87**, 109401, (2001).

18 Tcherbakov O *et al , Phys. Rev.* A **68 ,**043804,(2003)

19 Kovacev M *et al , Eur. Phys. J.* D **26 ,**79,(2003)

20 P. Tzallas *et al.*, *Nature*, **426**, 267, (2003).

21 Drescher M *et al , Science,* **291 ,**1923,(2001)

22 Hentschel M *et al, Nature,* **414,** 509,(2001)

23 Kienberger R *et al , Nature* **427 ,**817,(2004)

24 E. Papalazarou *et al., Phys. Rev. Lett.* **96**, 163901, (2006).

25 M. Shapiro *et al. Chem. Phys. Lett.* **149,** 451 (1988) ; Ce Chen *et al. Phys. Rev. Lett.* **64**, 507 (1990); A. D. Bandrauk *et al. Chem. Phys. Lett.* **200**, 399 (1992); T. Nakajima *et al. Phys. Rev. Lett.* **70**,1081 (1993); T. Nakajima *et al. Phys. Rev. A***50**, 595 (1993); E. Dupont *et al. Phys. Rev. Lett.* **74**, 3596 (1995); B. Sheehy *et al. Phys. Rev. Lett.* **74**, 4799 (1995); Langchi Zhu *et al. Science* **270**, 77 (1995); Langchi Zhu *et al. Phys. Rev. Lett.* **79**, 4108 (1997) ; S. Cavalieri *et al. Phys. Rev. A* **55**, 2941 (1997) ; D. Xenakis *et al. Optics Commun.* **152**, 83 (1998); N. E. Karapanagioti et al. *J. Phys.* B **29**, 3599 (1996) ; E. Charron *et al. Phys. Rev. Lett.* **71**, 692 (1993); E. Cormier *et al. J. Phys* B **30**, 3095 (1997) ; U. Andiel *et al. Europhys. Lett.* **47**, 42 (1999).

26 E. Hertz *et al.*, *Phys. Rev. A*, 64, 051801, (2001)

REFERENCES

27 E. Goulielmakis *et al.*, *Appl. Phys. B*, **74,** 197, (2002).

28 Berge Tatian, Applied Optics, **23**, 1984

29 Baron Jean Baptiste Fourier (see, e.g., http://bartleby.com/65/fo/Fouriers.html)

30 F. J. Harris, "On the Use of Windows for Harmonic Analysis with the Discrete Fourier Transform", Proc. IEEE, **66**(1), 51, (1978)

31 E. Goulielmakis *et al., Appl. Phys.* B **74**, 197, (2002).